Ore Geology Reviews 72 (2016) 546–561

Contents lists available at ScienceDirect

Ore Geology Reviews

journal homepage: www.elsevier.com/locate/oregeorev

High-grade ore shoots at the Martha epithermal vein system, Deseado Massif, Argentina: The interplay of tectonic, hydrothermal and supergene processes in ore genesis

G.N. Páez [a,b,*], R. Ruiz [a,c], D.M. Guido [a,b], F.J. Ríos [d], I. Subias [e], C. Recio [f], I.B. Schalamuk [a,b]

[a] Instituto de Recursos Minerales (INREMI), Universidad Nacional de La Plata Calle 64 esquina Calle 120, (1900) La Plata, Provincia de Buenos Aires, Argentina
[b] Consejo Nacional de Investigaciones Científicas y Técnicas (CONICET), Buenos Aires, Argentina
[c] YPF Tecnología (Y-TEC), Berisso, Argentina
[d] Laboratório de Inclusões Fluidas e Metalogênese, Centro de Desenvolvimiento da Tecnología Nuclear (CDTN-CNEN), Avenida Pres. Antônio Carlos 6627, Campus da UFMG, (31270-901) Belo Horizonte, Brazil
[e] Depto. de Ciencias de la Tierra, Universidad de Zaragoza, Edificio de Geológicas, Pedro Cerbuna 12, (50009) Zaragoza, Spain
[f] Servicio General de Isótopos Estables, Facultad de Ciencias, Plaza de la Merced s/n, (E-37008) Salamanca, Spain

ARTICLE INFO

Article history:
Received 13 March 2015
Received in revised form 27 July 2015
Accepted 30 July 2015
Available online 4 August 2015

Keywords:
Epithermal vein
Ore-shoot
Cooling
Dilution
Tectonic remobilization
Supergene enrichment

ABSTRACT

The complexity of high-grade ore-shoot formation is addressed through a detailed study of the Martha mine epithermal deposit (Deseado Massif, Patagonia, Argentina). The mine was active from 2002 to 2012, producing over 21 million oz of silver from an intermediate sulfidation vein system hosted in a pyroclastic sequence erupted during Upper Jurassic times (^{40}Ar–^{39}Ar age: 157.6 ± 1 Ma). The Martha deposit is composed of more than 15 different veins, 8 of which show high grade ore-shoots (locally up to 45,000 g/t Ag). Veins are hosted in a sinistral transtensive horst structure delimited by two NW–SE trending first-order veins (up to 600 m long and 5 m thick). Inside this horst, a series of E–W trending veins (up to 450 m long and 2.5 m thick) developed as second-order structures in response to growth and linkage of the two overlapping first-order vein structures. Ore is characterized by a complex paragenetic sequence of Ag–As–Sb sulfosalts and Cu–Pb–Zn sulfides, with an adularia-quartz-illite gangue. Hydrothermal alteration is zoned outward and rarely extends for more than 15 m away from the vein walls; five alteration zones were defined: an adularia zone close to the veins, an intermediate halo characterized by illite and illite–smectite zones, and a distal smectite zone, additionally a late and supergene kaolinite zone can be found near the surface in close association with the mineralized structures. High grade "bonanza" ore-shoots are the result of the interplay of a series of structural, hydrothermal (mostly physicochemical) and supergene processes. The mineralization evolved through three main phases: a main hydrothermal tectonically controlled phase, a late tectonic–hydrothermal phase and a post-mineral supergene phase. The main hydrothermal phase was the result of mineral deposition from low salinity (0.5 to 3.5 wt.% NaCl eq.) near-neutral to weakly alkaline chloride aqueous hydrothermal solutions with estimated temperatures ranging from 215.5 °C to 316.5 °C, and isotopic composition suggesting high proportions of meteoric waters ($\delta^{18}O_{H_2O}$ from −8.1‰ to −2.7‰). Relatively constant fluid inclusion liquid-to-vapor ratios and a trend of decreasing T_h and $\delta^{18}O_{H_2O}$ with increasing time suggest that cooling and dilution were the main mechanisms controlling ore deposition. These physicochemical conditions, combined with an efficient network of structural conduits (vein intersections, jogs and step-over zones) were the first step in the construction of the high grade ore shoots that characterize the vein system. ^{40}Ar–^{39}Ar dating in adularia crystals constrains the hydrothermal activity to the Upper Jurassic (156.5 ± 0.9 Ma). Afterwards, a late tectonic–hydrothermal phase occurred through the development of irregularly-shaped bodies of massive fault breccias and foliated cataclasites related to tectonic reactivations of the vein system in synchronism with the waning stages of the hydrothermal system. The interplay between deformation and fluid circulation resulted in mechanical and chemical remobilization of the previously deposited Ag-rich sulfosalts by lower temperature (138 °C to 168 °C) and higher salinity fluids (7.7 and 9.9 wt.%. NaCl eq.), possibly reflecting a late magmatic input into the waning system. This late tectonic–hydrothermal phase strongly contributes to increase the grades in some veins, and therefore is considered an essential process in order to build the highest-grade portions of the ore-shoots found at the mine. Finally, a post-mineral supergene phase defined a 20 m thick oxidized zone close to the surface, followed by a 20–30 m thick secondary enrichment zone below it, developed in response to the circulation of descending cold meteoric waters. Despite its small size and vertical extension, the secondary enrichment level at Martha mine constitutes an important economic factor for the mining

* Corresponding author at: Instituto de Recursos Minerales (INREMI), Calle 64 esquina calle 120, (1900) La Plata, Provincia de Buenos Aires, Argentina.
E-mail address: gerardo.paez.unlp@gmail.com (G.N. Páez).

http://dx.doi.org/10.1016/j.oregeorev.2015.07.026

operations as it helped to increase the silver grades in the shallower portion of the vein system. The Martha mine vein system constitutes an excellent example of how the interplay of hydrothermal processes controlling mineral deposition, structural factors building up an efficient plumbing system, tectonic ore-remobilization, and late supergene secondary enrichment processes, are combined in order to build "bonanza"-grade ore shoots in the epithermal environment.

1. Introduction

In this paper, the complexity of high-grade ore-shoot formation in the epithermal environment is addressed (Hedenquist et al., 2000; Sillitoe and Hedenquist, 2003; Simmons et al., 2005) through a detailed study of the Martha mine epithermal deposit, located in the southwestern portion of the Deseado Massif, Southern Patagonia, Argentina (Fig. 1a). The vein system was first discovered by Yamana Resources Inc. in 1997 and mining operations started at 2001, during early 2002 the mine was bought by Coeur d'Alene Mines Corporation and was in production until 2012 (Figs. 1b and 2a) when the resources were completely mined out. Currently the mine remains closed and no exploration has been conducted since late 2012. Silver concentrations were very high grade, such that in 2002 the mine was ranked 15th among the world's silver producers (www.silverinstitute.org). It has produced more than 21 million oz of silver (more than 50% of the Deseado Massif's total silver production) and over 28,000 oz of gold, with an average grade of about 3500 g/t Ag and almost 5 g/t Au (Páez, 2012).

Previous studies of Páez et al. (2011) and Páez (2012) at the Martha mine showed a close relationship between high grade ore shoots and the location of structural features (vein intersections, dilatational jogs and step-overs), suggesting that structure played a significant role during ore-shoot formation, controlling preferential pathways for hydrothermal solutions, leading to ore deposition.

However, the presence of highly permeable conduits per se is insufficient to lead to high grade "bonanza" mineralization. The interplay of those structures with an efficient ore deposition mechanism is considered critical in order to form an economic-grade deposit (Simmons and Browne, 2000; Berger et al., 2003; Cox, 2005; Simmons and Brown, 2006; Micklethwaite, 2009).

This research complements the observations of Páez et al. (2011) by giving new insights into the study of the vein infills with the aim to constrain the physicochemical processes leading to the formation of high-grade "bonanza" style ore-shoots in the epithermal environment. We combine field, underground and drill-hole observation with mineralogical, textural, microthermometric, isotopic and geochronological

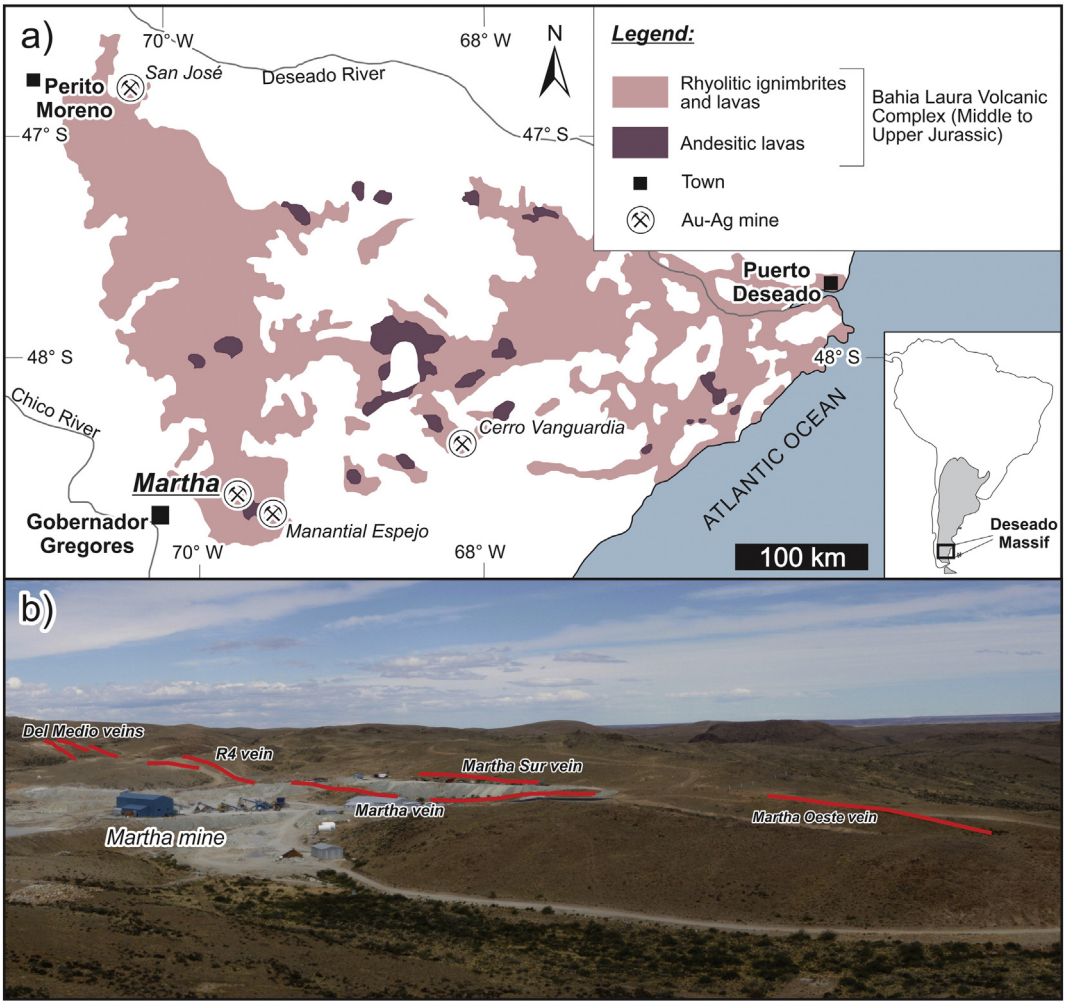

Fig. 1. a) Simplified geological map of the Deseado Massif showing distribution of Jurassic volcanic rocks and the location of the four mine sites mentioned in the text. b) Photo looking south at the Martha mine operations area showing the location the studied veins.

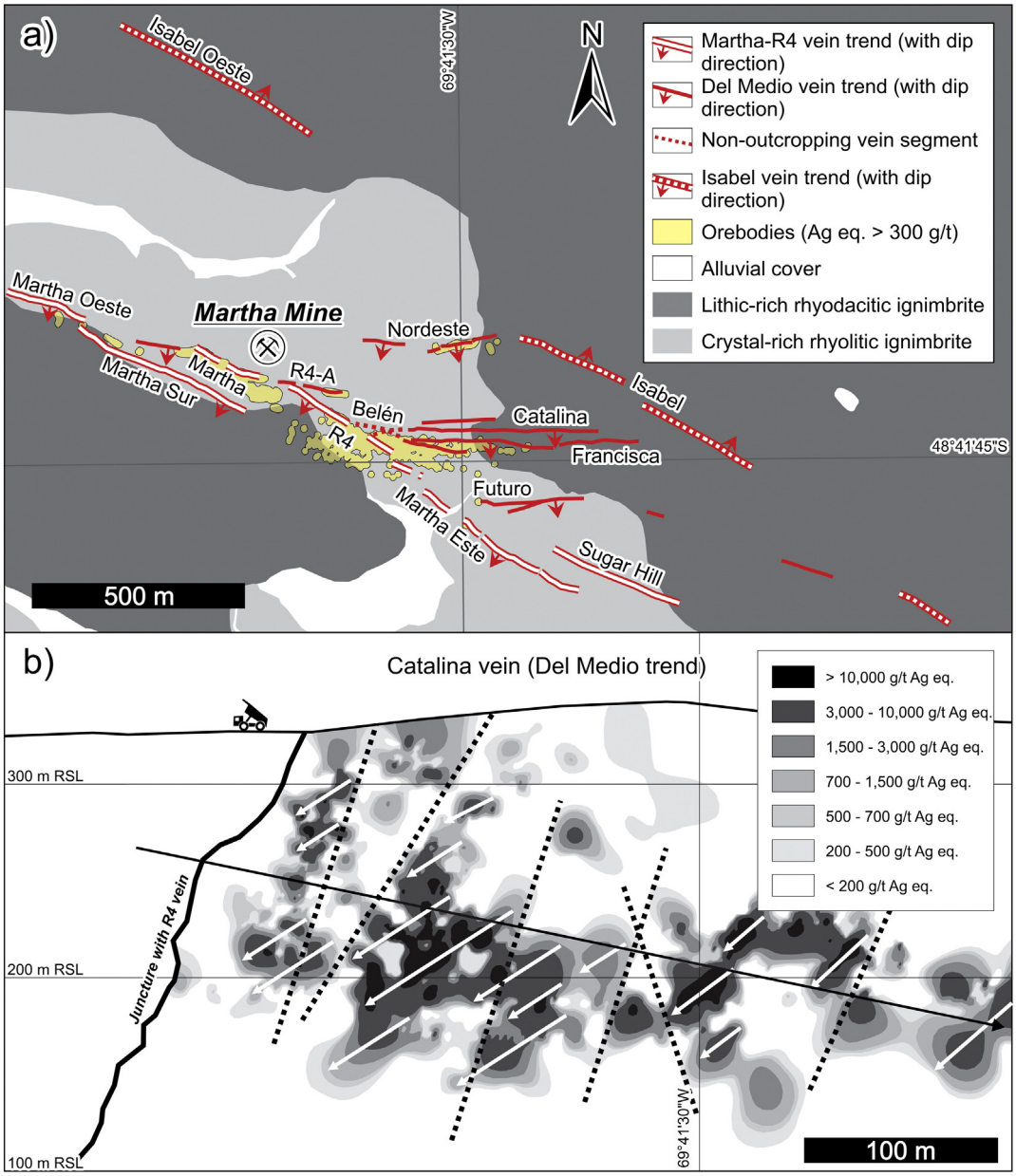

Fig. 2. a) Geological map of Martha mine vein system showing the location of the main vein trends and the vertical projection of mineralized areas (Ag equivalent > 300 g/t). b) Longitudinal section of Catalina vein (del Medio trend) showing Ag equivalent grades. The plunge of the first order ore-shoot is represented by a black arrow, whereas second order ore-shoots are shown by white arrows. Dashed lines represent post-mineral faults dislocating ore-shoots. Altitude is in meters with respect to sea level (m RSL). In both cases Ag equivalent = (Ag + 60*Au), modified from Páez et al. (2011).

data obtained on selected samples, in order to propose a comprehensive model of vein and ore-shoot formation.

2. The Deseado Massif

2.1. Regional geology

During the Middle to Upper Jurassic, a volcanic mega-event occurred in Patagonia, giving rise to the Chon Aike Large Igneous Province (Pankhurst et al., 1998, 2000). In the Deseado Massif (Fig. 1a), this event is represented by a volcanic suite that was named the Bahía Laura Volcanic Complex (BLVC) by Feruglio (1949) and Guido (2004), and consists of the Bajo Pobre, Cerro León, Chon Aike and La Matilde formations, including lavas, ignimbrites and reworked volcaniclastic rocks ranging from intermediate to acidic in composition (Pankhurst et al., 1998, 2000; Panza and Haller, 2002). Intricate stratigraphic relationships characterize this volcanic complex, with complex interfingering of different facies (Echeveste et al., 2001; Guido et al., 2006; Ruiz, 2012).

2.2. Mineral deposits

This region is characterized by numerous gold and silver epithermal deposits, leading Schalamuk et al. (1999) to define the Deseado Massif as an Au–Ag metallogenic province. Most Au–Ag occurrences within the Deseado Massif correspond to the low sulfidation style (Guido and Schalamuk, 2003; Echavarría et al., 2005; Fernández et al., 2008), however intermediate sulfidation and polymetallic deposits are also common (González Guillot et al., 2004; Guido, 2005; Jovic et al., 2011; Páez, 2012; Permuy Vidal, 2014). These deposits are commonly hosted in the BLVC rocks, mainly in the Chon Aike and Bajo Pobre Formations;

however there are also epithermal occurrences in older pre-BLVC rocks of sedimentary or metamorphic nature (Jovic et al., 2011).

The typical mineralization style consists of veins, veinlets, vein stockworks and hydrothermal breccias (Schalamuk et al., 1997, 1999; Guido and Schalamuk, 2003), which are strongly controlled by Jurassic rift structures, hosted in dominant NW and WNW orientations, and locally in NE and E–W directions (Giacosa et al., 2010). Associated with the epithermal veins, widespread silica and carbonate Jurassic hot spring deposits are present (Guido and Campbell, 2011). Available geochronological data reveals that epithermal veins and hot spring deposits were formed during the Jurassic widespread extensional event, contemporaneous with the last stages of the BLVC event (Arribas et al., 1996; Schalamuk et al., 1997; Guido and Schalamuk, 2003; Echavarría et al., 2005).

According to Fernández et al. (2008) and Páez et al. (2011), between 1998 and 2011 the Deseado Massif has produced more than 3 million oz of gold and over 40 million oz of silver from four mines (Cerro Vanguardia, Martha, Manantial Espejo and San José; Fig. 1a). Most of the precious metals have been extracted from Cerro Vanguardia mine (about 77%, beginning in 1998), followed by 11% from Martha mine (producing between 2001 and 2012), and the remaining 12% from San José and Manantial Espejo mines (producing since 2008 and 2009, respectively), revealing the importance of Martha mine in the overall precious metal production of this relatively young gold and silver producing region.

3. Local geology

The mineralization at Martha mine is hosted in Jurassic felsic volcanic rocks of the BLVC that are locally represented by thick ignimbrites (Figs. 1 and 2) with thin intercalations of epiclastic sediments derived from a pyroclastic source (tuffites). In total, mineralization extends across a 300 m-thick volcanic pile, located about 2–3 km southward of the of Primero de Abril Caldera margin (Ruiz et al., 2008a, 2008b; Páez et al., 2010; Ruiz, 2012), a 10 km wide volcanic edifice resulted from mixing of two magmas of andesitic and rhyolitic compositions during Upper Jurassic Times (156.9 ± 0.7 Ma; Ruiz, 2012).

The oldest geological unit in the study area is represented by a crystal-rich dacitic ignimbrite, which is overlain by a thin tuffaceous unit (Páez et al., 2010). Upwards in the sequence there is a crystal-rich rhyolitic ignimbrite followed again by a thin layer of tuffaceous sediments. The upper part of the sequence is composed of a lithic-rich rhyodacitic ignimbrite related to the caldera-forming volcanic event. The entire sequence dips about 10° toward the NE (Páez et al., 2010). Most of the high grade ore bodies are developed in the crystal-rich ignimbrites and tuffaceous units (Páez, 2012).

All pyroclastic rocks at Martha mine are characterized by a calcalkaline, peraluminous and high potassium signature (Páez et al., 2010; Páez, 2012; Ruiz, 2012), in concordance with other reported areas of the BLVC (Pankhurst et al., 1998; Guido, 2004). Regional studies performed by Echeveste (2005), Wallier (2009) and Ruiz (2012) indicates that outside the Martha mine area, the described sequence is partly buried by younger Jurassic units (mostly ignimbrites and lavas), tertiary marine sediments and modern alluvial to colluvial sediments.

4. The Martha mine vein system

The Martha deposit is composed of more than 15 different veins, 8 of which show high grade ore-shoots (locally up to 45,000 g/t Ag, Páez et al., 2011): Martha, R4, Nordeste, R4-A, Catalina, Francisca, Belén and Isabel (Fig. 2a).

4.1. Vein system and ore shoot geometry

The Martha mine veins can be grouped into three major vein trends according to their general orientation and location (Fig. 2a). First, the NW–SE trending Martha–R4 vein trend (including Martha Oeste, Martha, R4, Martha Este, Martha Sur and Sugar Hill veins); second, in a parallel array but toward the northeast, the Isabel vein trend (including Isabel and Isabel Oeste veins); and third, the Del Medio vein trend grouping all the E–W trending veins (including Nordeste, R4A, Belén, Francisca, Catalina and Futuro veins).

The Martha–R4 vein trend is characterized by a moderately SW dipping segmented array with an overall NW–SE orientation (Fig. 2). The vein trend is composed of a single 1.5 to 5 m thick structure made of a dense network of anastomosing veins and veinlets, partially developed within a 10 m thick clay-rich (gouge) fault zone. This structure can be followed long strike for 600 m in a series of discontinuous outcrops, and mineralization has been reported down to depths of about 250 m below the surface (Páez et al., 2011; Páez, 2012). Limited surface (open-pit) and widespread underground workings have been conducted on this vein trend, especially in high grade portions of the Martha and R4 veins.

The Del Medio vein trend constitutes a subparallel array of steeply south dipping E–W trending structures (Fig. 2), ranging between 0.5 and 1 m thick and which locally can reach up to 2.5 m, and is characterized mostly by tabular geometries. This vein trend extends 150 to 450 m along strike, and mineralization is reported down to depths of about 200 m below the surface (Páez et al., 2011; Páez, 2012). Underground mining have been conducted on Francisca, Catalina, Belén veins; whereas R4-A and Nordeste veins were mined out using both underground and surface workings.

The Isabel vein trend is made of two NE dipping disconnected vein segments with a NW–SE orientation (Fig. 2). Only minor underground workings were developed in these veins, which have poor grades and crop out infrequently (Páez et al., 2011; Páez, 2012).

Structural studies at Martha mine (Páez et al., 2011) suggest that the vein system was emplaced in a sinistral transtensive horst structure delimited by the Martha–R4 and Isabel vein trends (Fig. 2a). Within this model, the geometries of the three main vein trends where interpreted as a hard-linked extensional step-over, where the Del Medio vein trend developed as second-order structures in response to growth and linkage of two overlapping, first-order structures composed of the Martha–R4 and Isabel vein trends (Fig. 2a). Geometric analyses of Martha mine veins also showed a normal-sinistral slip kinematic mode, with an associated opening component for all considered structures; in addition, the geometry of ore-shoots at Martha mine suggests a first-order structural control on their location and orientation (Páez et al., 2011).

On this structural framework, ore-shoot geometry was also described by Páez et al. (2011), who defined them as irregular and discontinuous silver-rich bodies that can reach very high grades (up to more than 45,000 g/t Ag and up to 170 g/t Au). At the deposit-scale, a series of several hundred meters long ore bodies are observed within the hard-linked extensional step over zone, in close affiliation with vein intersections (Fig. 2a). Within single veins, mineralization is represented as broad areas defining gently plunging first order ore-shoots of irregular shapes (black arrow in Fig. 2b), which are a result of the combination of numerous high grade second order ore-shoots (white arrows in Fig. 2b). First order ore-shoots are developed as broad areas extending almost the entire length of the veins (Fig. 2b). They typically have surfaces exceeding 15,000 m^2 and are dominated by medium to high silver grades. However, they are quite irregular in shape and include some low grade portions. These ore-shoots are characterized by a very gentle plunge of less than 10° toward the SE. Second order ore-shoots are smaller, extending between 10 and 70 m along the vein strike (Fig. 2b), commonly they show surface areas not exceeding 2500 m^2, and are defined by the high grade portions of the first order ore-shoots. These shoots form the highest grade bodies (Fig. 2b), which plunge 30° to 40° toward the SW, and can be individually associated with dilatational jogs and step-over zones developed within veins (Páez et al., 2011).

4.2. Vein geochemistry

Statistical analysis of geochemical data from 1553 drill-core samples shows that Martha mine veins are characterized by strong silver contents with associated gold anomalies. Statistical analysis indicates a mean precious metal content of 3500 ppm Ag and 5 ppm Au, with a strong correlation between Ag and Au grades ($R^2 = 0{,}9$), and a mean Ag/Au ratio of about 900:1. Maximum grades may rise up to 45,000 ppm Ag and 170 ppm Au within high grade ore shoots (Páez et al., 2011; Páez, 2012). Additionally, silver values show a strong correlation with Sb contents ($R^2 = 0{,}8$) which show an average content of 0.2% Sb. Precious metals are accompanied by base metals, with mean values of 0.14% Cu, 0.2% Pb and 0.12% Zn, and maximum contents of about 0.94% Cu, 0.68% Pb and 0.22% Zn. Moreover, anomalies of As, Hg, Bi and Cd can be locally recognized within the veins.

5. Hypogene vein mineralogy and textures

The mineralized structures at Martha were developed under a complicated history of fracturing and cementation (Páez et al., 2011; Páez, 2012). Nine mineralizing pulses (stages) of primary origin were identified based on their crosscutting relationships, and were grouped into four main episodes based on the presence or absence of ore minerals in their mineral assemblage (Fig. 3).

5.1. Vein paragenesis

5.1.1. Episode 1

This episode (E1, Fig. 3a) includes the barren pre-ore stage 1, which is poorly represented within the deposit. This stage is made of a network of thin 0.5 mm thick veinlets, of sacharoidal quartz with minor sub-rhombic adularia (Dong and Morrison, 1995) and no associated ore minerals except for traces of pyrite and arsenopyrite.

5.1.2. Episode 2

The second episode (Fig. 3a) comprises four stages with a progressively decreasing sulfide content, ranging from a massive sulfide stage (stage 2, Fig. 3b) to a sulfide poor stage (stage 5, Fig. 3c). This episode is responsible for part of the high grade ore and contains silver and base metal bearing sulfides and sulfosalts. Gangue minerals of this episode are adularia, quartz and minor illite. It typically has a brecciated texture; with locally developed crustiform banding.

Stage 2 consists of coarse-grained sulfides with no associated gangue minerals (Fig. 3a–c), and marks the onset of the first sulfide-bearing episode. Stage 2 is characterized by the deposition of coarse-grained pyrite (up to 1 cm wide) carrying numerous sulfide and sulfosalt inclusions (Figs. 3a, 4a and b), with both regular and irregular distribution patterns (Fig. 4a). In both cases, the inclusions are mostly galena, polybasite, acanthite and native silver (Figs. 3a and 5b), with minor chalcopyrite (Figs. 3a and 5a), pyrargyrite and arsenopyrite. This stage can be found both as massive veins or breccias, and also as clasts within later stages in most mineralized structures. Additionally, within the Del Medio vein trend, this stage can also be found as part of a crustiform banding along with stages 3 and 4 (Fig. 4b and c).

Stage 3 is characterized by a high sulfide and sulfosalt content (commonly around 50 vol.%) in a mosaic-like intergrowth with sub-rhombic adularia (Dong and Morrison, 1995) and anhedral to subhedral quartz, with minor illite (Figs. 3a and 4c). This stage displays a medium to fine-grained massive texture commonly with host rock and stage 2 clasts; also it may form part of a crustiform array along with stages 2 and 4 in the Del Medio vein trend (Fig. 3b). Ore mineral deposition starts with an intergrowth of galena and sphalerite with associated chalcopyrite, arsenopyrite, polybasite and native silver (Figs. 3a and 4d). Later on this stage, chalcopyrite contents increases, crosscutting and replacing previously deposited mineral phases, especially galena and sphalerite.

Sulfide and sulfosalts contents on stage 4 are commonly around 30 vol.%, but locally can reach up to 50 vol.%, and are developed in an intimate mosaic-like intergrowth along with gangue minerals (Figs. 3b, 4e and f). This stage is typically massive and may include host rock, stages 2 and 3 clasts; and in some cases it may form the central band of crustiform veins along with stages 2 and 3, especially within the Del Medio vein trend. Gangue minerals are represented by sub-rhombic adularia, anhedral to subhedral quartz, minor illite and traces of chlorite (Figs. 3a and 4e). Gangue mineral deposition starts with a slightly higher content of sub-rhombic adularia compared to quartz; however this proportion changes toward the end of this stage, where the quartz content is slightly higher, and small drusy cavities can be observed.

Ore minerals are represented by a complex sulfide and sulfosalt assemblage (Figs. 3a and 4f) represented by widespread Ag-bearing tetrahedrite, sphalerite, galena, chalcopyrite and pyrite, with subordinated amounts of Se-rich polybasite (Márquez-Zavalía et al., 2008), miargyrite, pyrargyrite, freieslebenite, native silver, acanthite and minor arsenopyrite. In most cases, tetrahedrite crystals are typically replaced by a rim of chalcopyrite and acanthite toward the edges, suggesting high contents of silver within the tetrahedrite. Finally, two pyrite generations can be recognized, an early-stage pyrite characterized by subhedral and inclusion-free crystals (Fig. 4f) and a late-stage pyrite formed as a replacement over tetrahedrite, and characterized by minute inclusions of tetrahedrite, acanthite and/or native silver all of them showing vermicular textures.

Stage 5 is mostly comprised of gangue minerals, whereas ore mineral contents typically range between only 5 and 10 vol.% (Fig. 3a and c). This stage is made of a medium-grained intergrowth of sub-rhombic adularia, subhedral to euhedral quartz and traces of illite (Figs. 3a and 4g), with a massive texture that may include several clasts of the host rocks and/or previous stages.

Gangue mineral deposition starts with a high proportion of adularia, minor quartz and no ore minerals (Fig. 3a and c). Later on in this stage, the adularia contents decrease whereas the quartz increases along with the contents of sulfides and sulfosalts (Fig. 3a and c). These changes may occur both as a progressive increase in the quartz/adularia proportion, or it can be defined by a relatively sharp change (as the case of Fig. 3c). Finally, small drusy cavities lined with amethyst can be observed on the quartz-rich portions of this stage.

Ore minerals are typically late and interstitially developed among the gangue minerals (Fig. 4g and h). Sulfides and sulfosalts are represented mostly by miargyrite and acanthite with associated arsenopyrite, chalcopyrite, and traces of galena and sphalerite (Figs. 3a and 4h).

5.1.3. Episode 3

The third episode (Fig. 3a) is composed of two barren stages characterized by massive adularia (stage 6, Fig. 3d and e) and quartz with minor adularia (stage 7, Fig. 3e). These stages are typically massive to brecciated in texture and widespread among all veins, in most cases building up to the 95 vol.% of the veins, especially stage 6.

Stage 6 is the volumetrically most important stage within the Martha mine vein system, building up to 95 vol.% of most veins (up to 1.5 m in thickness); it consists of a sulfide-free assemblage of coarse-grained adularia (up to 1 cm long) with minor amounts of quartz (Fig. 3a, d and e). Tabular euhedral to subhedral adularia (Fig. 5a, Dong and Morrison, 1995) represents almost 80 vol.% of this stage and is best developed as an early-stage mineral phase (Fig. 3a). On the other hand, quartz and amethyst are typically late within this stage (Fig. 3a), tending to concentrate toward the center of the structures, and showing comb, zoned and feathery textures (Fig. 5b, Morrison et al., 1995). Additionally, large drusy cavities up to 30 cm in diameter can be recognized in the central portions of this stage with several centimeter long quartz and amethyst crystals.

Stage 7 consists of a poorly represented network of anastomosing veinlets (Fig. 3a and e) containing a fine-grained intergrowth of

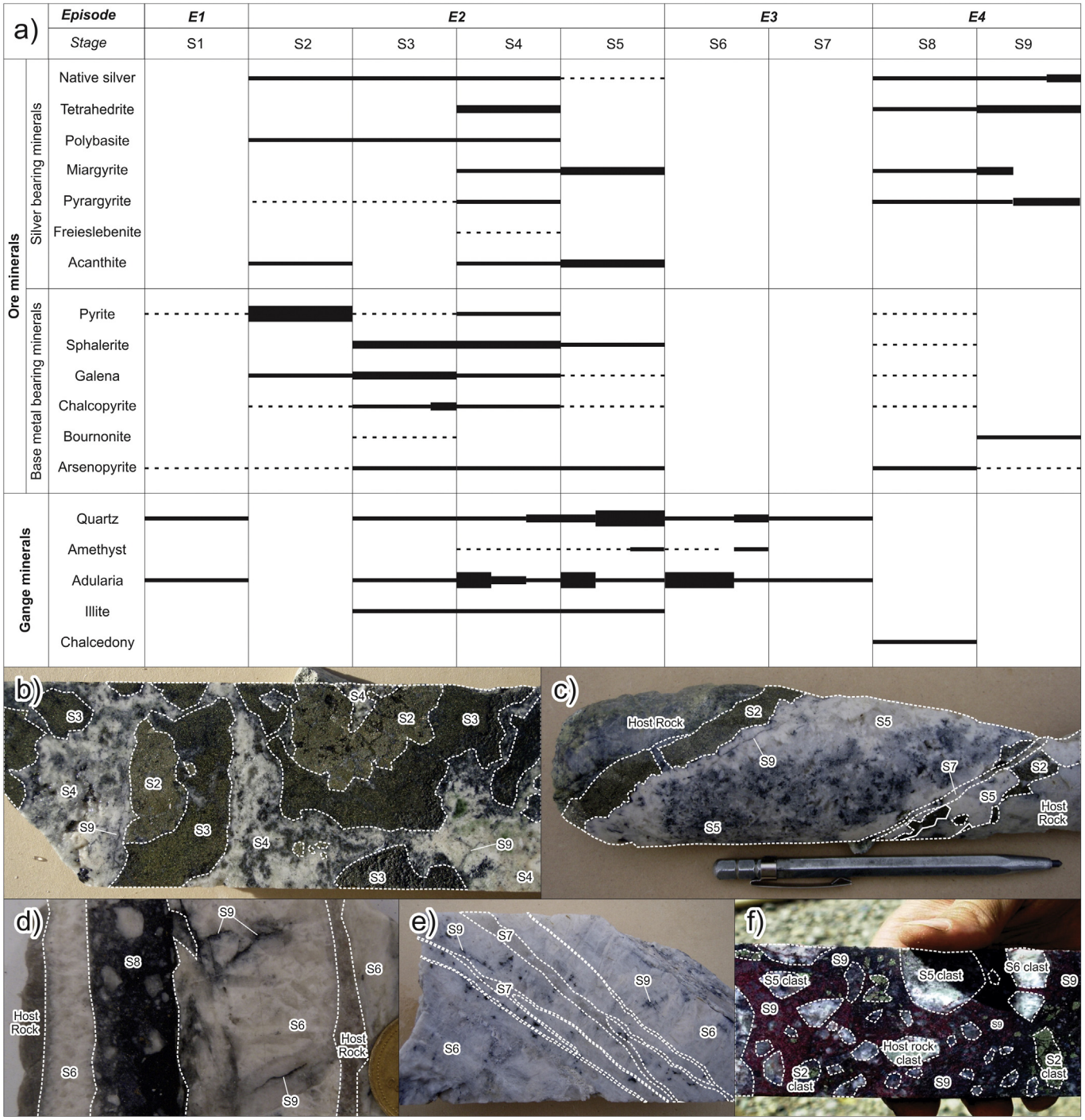

Fig. 3. a) Paragenetic diagram of ore-gangue minerals at the Martha mine vein system. b) Textures and crosscutting relationships between stages 2, 3 and 4 at Catalina vein (Sample Id: P.Cata-A; Drill-hole M-512 at 188.5 m; Ag grade: 10,602 ppm). c) Textures and crosscutting relationships among stages 2, 5, 7 and 9 at Belén vein (Sample Id: 11301; Drill-hole M-259 at 174.5 m; Ag grade: 12,595 ppm). d) Hand specimen of R4 vein with crosscutting relationships between stages 6, 8 and 9 (Sample Id: 10689, underground workings at 215 level; Ag grade: not available). e) Drill-hole sample of Catalina vein showing crosscutting relations between stages 6 and 7 (Sample Id: 10324; Drill-hole M-512 at 188.5 m; Ag grade: 1026 ppm). f) Detailed view of stage 8 breccias in R4 vein (Sample Id: R4-524; Drill-hole M-524 at 187.2 m; Ag grade: 47,463 ppm), the reddish to purple color of the matrix is due to the presence high amounts of pyrargirite.

sacharoidal quartz, rhombic adularia and minor illite (Fig. 5c and d), with no associated ore minerals.

5.1.4. Episode 4

The fourth and last primary episode (Fig. 3a) is characterized by two late stages, composed by discontinuous chalcedonic breccias with a highly variable sulfide content (stage 8, Fig. 3d and f), and a system of thin sulfide veins that can locally build up to a dense network (stage 9, Fig. 3b–d). This episode has a widespread distribution between Martha and R4 veins, but is commonly absent among the E–W trending veins. This final episode, despite its late nature, can become an important component of the high grade ore shoots as it strongly contributes to the grades of the mineralization (Páez et al., 2011).

Stage 8 consists on irregularly-shaped bodies of a massive cohesive fault breccia (Passchier and Trouw, 2005), with angular to subangular clasts, surrounded by a fine-grained silicified milled matrix (Figs. 3d, f,

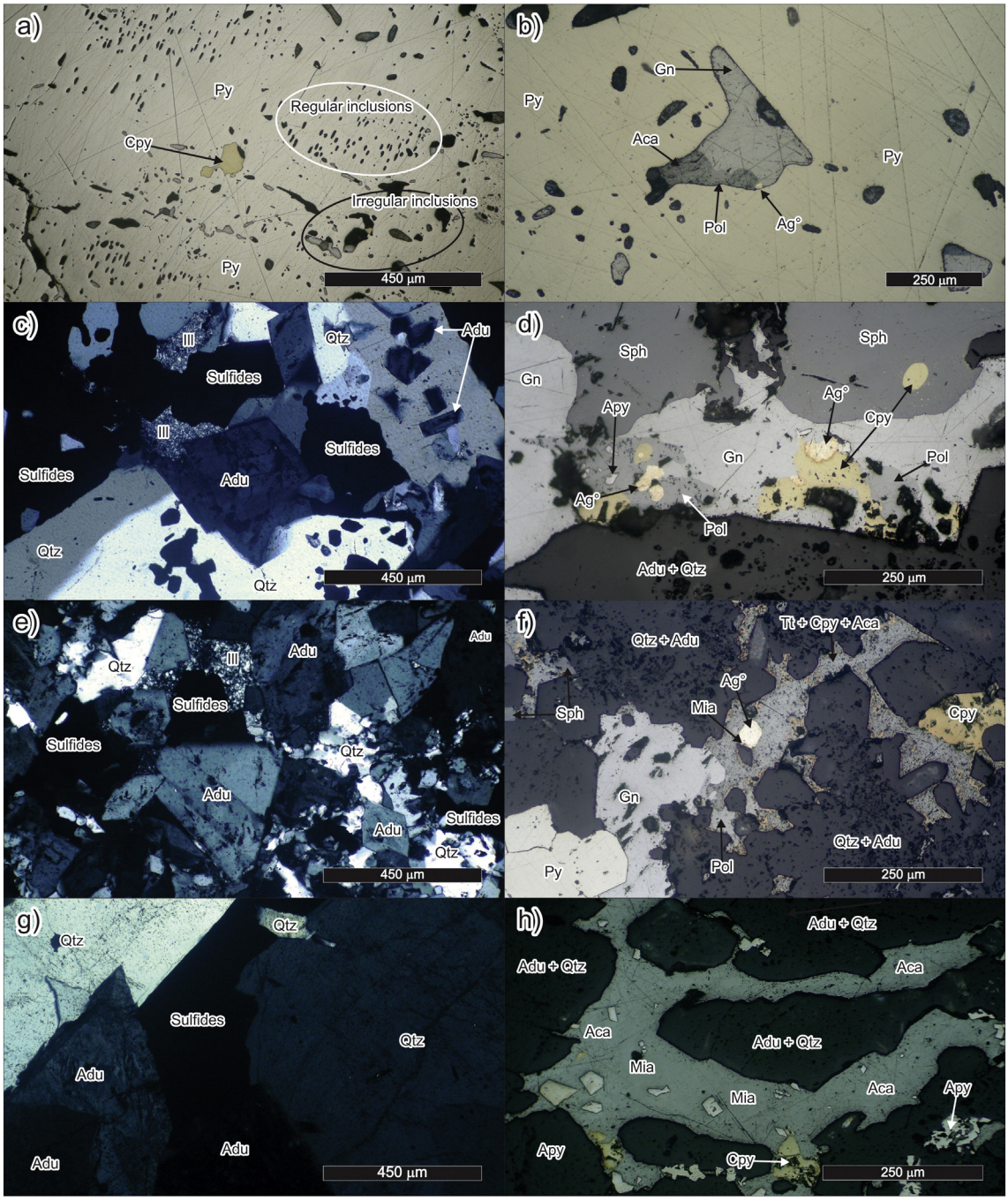

Fig. 4. Ore and gangue mineralogy and textures of mineralizing episode 2 viewed under the polarizing microscope. a) Stage 2: coarse-grained pyrite crystals carrying regular and irregular sulfide and sulfosalt-rich inclusions. Reflected light. b) Stage 2: pyrite-hosted irregular inclusion of galena, acanthite, polybasite and native silver. Reflected light. c) Stage 3: gangue assemblage of subrhombic adularia, quartz and illite with opaque ore minerals. Transmitted light, crossed polarizers. d) Stage 3: intergrowth of galena, sphalerite and chalcopyrite with polybasite and native silver. Reflected light. e) Stage 4: mosaic texture of subrhombic adularia, quartz and illite with opaque ore minerals. Transmitted light, crossed polarizers. f) Stage 4: intergrowth of galena, pyrite, chalcopyrite and sphalerite with tetrahedrite, native silver and miargyrite. The tetrahedrite crystals show an overgrowth of chalcopyrite and acanthite. Reflected light. g) Stage 5: coarse-grained sub-rhombic adularia and quartz with interstitially developed ore minerals (opaque). Transmitted light, crossed polarizers. h) Stage 5: intergrowth of miargyrite (with less scratches), acanthite (with more scratches) and minor chalcopyrite and arsenopyrite. Reflected light. Abbreviations: Aca = acanthite, Adu = adularia, Ag° = native silver, Apy = arsenopyrite, Cpy = chalcopyrite, Gn = galena, Ill = illite, Mia = miargyrite, Pir = pyrargirite, Pol = polybasite, Py = pyrite, Qtz = quartz, Sph = sphalerite, Tt = tetrahedrite.

5e and f). Clasts typically show a large variability in size, ranging in diameter from decimeter down to millimeter scales (Figs. 3d, f and 5e). In some cases, these breccias transitionally grade into foliated cohesive cataclasites (Passchier and Trouw, 2005), showing smaller clast sizes and a higher proportion of matrix material (Fig. 5f). In this case the foliation is usually enhanced by the presence of sulfides/sulfosalts.

When crosscutting previous mineralizing stages, the breccia bodies are characterized by the presence of large quantities of clasts from previous stages and minor host rock clasts, surrounded by a dark to reddish colored matrix (Fig. 3f), due to the presence of a new generation of abundant silver sulfosalts. When this occurs, the breccias tend to show high to very high silver grades, typically well above 1500 ppm Ag. However, when these breccias crosscut only host rocks with no significant mineralization, clasts are mostly monolithologic in nature, and made exclusively of the ignimbritic sequence that hosts the mineralization. When this happens, the matrix is commonly light gray in color and

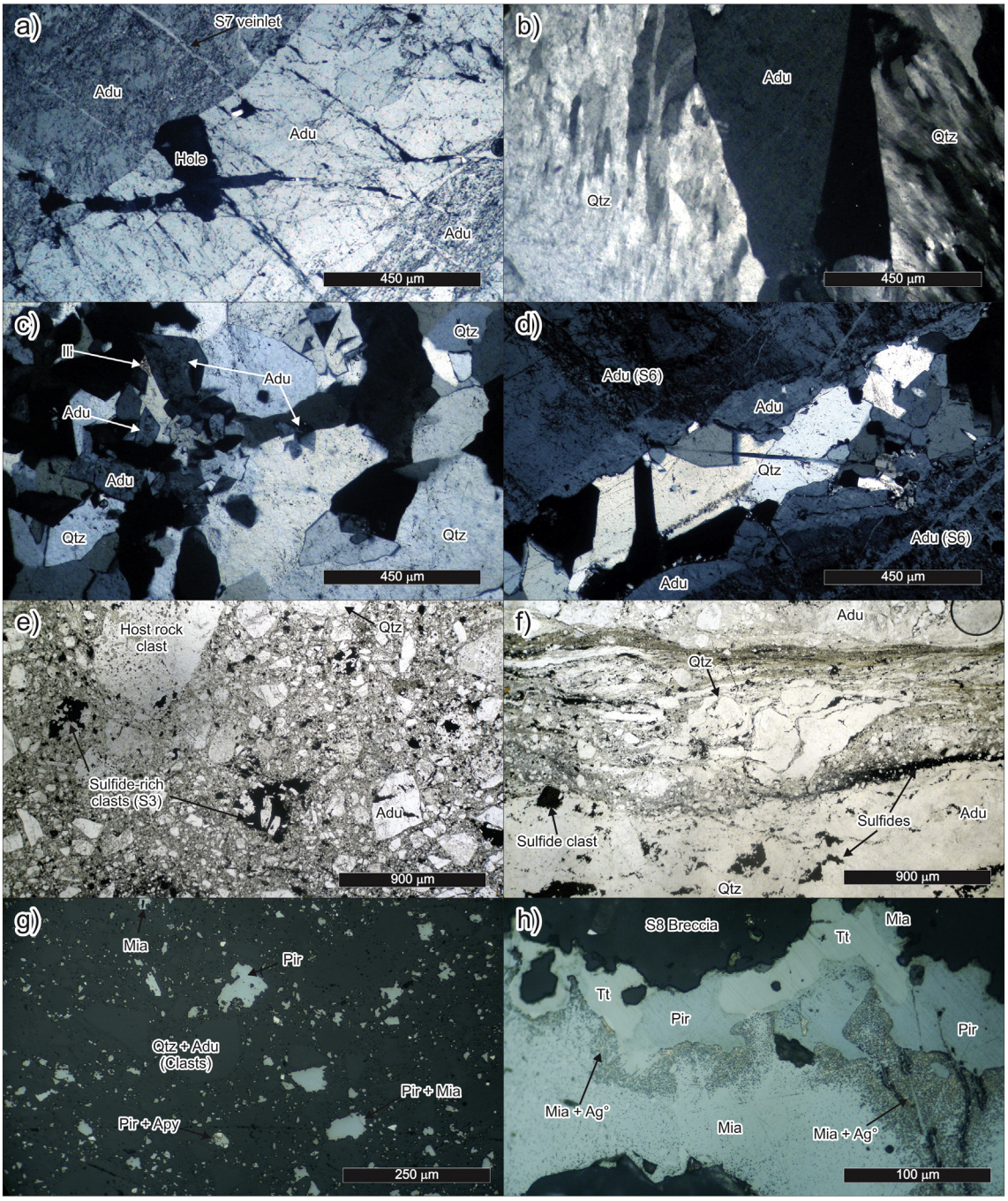

Fig. 5. Ore and gangue mineralogy and textures of mineralizing episodes 3 and 4 viewed under the polarizing microscope. a) Stage 6: coarse-grained tabular adularia with crosscutting stage 7 veinlets. Transmitted light, crossed polarizers. b) Stage 6: coarse-grained plumose quartz and tabular adularia. Transmitted light, crossed polarizers. c) Stage 7: mosaic texture made of quartz and rhombic adularia. Transmitted light, crossed polarizers. d) Stage 7: Stage 6 tabular adularia cut by a stage 7 veinlet made of quartz and rhombic adularia. Transmitted light, crossed polarizers. e) Stage 8: massive fault breccia with E2 and host rock clasts in a milled matrix. Transmitted light, parallel polarizers. f) Stage 8: foliated cataclasite with quartz and sulfide clasts in a milled foliated matrix. Opaque minerals (sulfides) tend to enhance the foliation by alignment of grains. Transmitted light, parallel polarizers. g) Stage 8: pyrargirite and miargyrite filling cavities within the breccias. Reflected light. g) Stage 9: veinlet infill consisting of pyrargyrite, miargyrite tetrahedrite and native silver. Abbreviations as in Fig. 4.

exhibits very low silver grades (normally barren); however, silver grades progressively increases when the breccias approach the mineralized zones of the vein trend (Páez et al., 2011).

In this stage, previous mineralizing stages are present as fractured sulfide and sulfosalt-rich clasts, commonly with evidences of cataclasis. Newly formed sulfides (mostly arsenopyrite, pyrite, sphalerite, chalcopyrite and galena, Fig. 3a) are generally developed as overgrowths or healing fractures over previous sulfides. Moreover, high grade areas are dominated by the widespread development of newly formed silver and copper bearing sulfosalts (Figs. 3a and 5g), mostly pyrargyrite, miargyrite and Ag-bearing tetrahedrite, infilling small irregular cavities within the breccia matrix (Fig. 5g). Gangue minerals are mostly absent, with the exception of minor chalcedony on the breccia matrix.

Stage 9 consists of a discontinuous network of thin veinlets, up to 2 mm thick, containing of silver and copper sulfosalts (Fig. 3a, c and d). This stage is closely associated with stage 8 breccias, and therefore is unlikely to be found when stage 8 is absent. Gangue minerals are absent within this stage (Fig. 3a), and ore minerals are characterized by an irregular intergrowth of silver and copper sulfosalts (Figs. 3a and 5h), mostly pyrargyrite and miargyrite, with associated Ag-bearing

tetrahedrite, native silver and minor amounts of bournonite and arsenopyrite. Additionally, pyrargyrite and miargyrite may be also present as a myrmekitic intergrowth, and native silver may be present as minute inclusions within miargyrite crystals, especially toward the crystal borders (Fig. 5h).

6. Supergene ore modifications

Studies of the vein mineralogy, textures and geochemistry demonstrate that the shallowest portions of the Martha vein system have been affected by oxidation and secondary enrichment, as noted by Páez (2012).

The metal ratio (Ag/Au) vs. depth profile shows a shallow 20 m thick oxidation zone (Fig. 6a) dominated by a maximum Ag/Au value of about 2000:1 (with a mean value of 800:1); this shallow portion of the deposit is also characterized by higher Pb contents along with lower Cu and Zn grades, with respect to the primary zone. The ore mineral association of the oxidized zone is characterized by native silver, limonites, jarosite, plumbojarosite [$PbFe_6(SO_4)_4(OH)_{12}$], chlorargyrite–embolite [Ag(Br,Cl)], boleite [$KPb_{26}Ag_9Cu_{24}Cl_{62}(OH)_{48}$], cerussite, malachite and azurite. This assemblage is recognized usually as thin veinlets and/or as cavity infill within the vein (Fig. 6b).

Below the oxidized zone, a 20–30 m thick enrichment zone can be recognized by a sharp increase in the maximum value of the Ag/Au ratio (up to 20,000:1, Fig. 6a); this change is followed by an increase in Cu and Zn grades, and a progressive reduction in Pb contents. This zone is typically dominated by acanthite (Ag_2S), pyrargyrite, native silver, chalcocite, digenite, covellite, and minor bornite and spionkopite [$Cu_{1,4}S$]. These minerals can be identified partially replacing the primary sulfides (Fig. 6c), forming thin veinlets, or also as small cavity infill.

Downwards, the enrichment zone grades into the primary mineral association (Fig. 3a). This transition is defined by a progressive reduction in the Ag/Au ratio (Fig. 6a) to values as high as 4500:1 (with a mean of 1000:1), Cu and Zn values are also lower but remaining higher than in the oxidized zone; finally, Pb values reach the lowest values in the profile.

7. Hydrothermal alteration

The extent and intensity of the alteration halo is closely related to the proximity and to the magnitude of the mineralized structures, however strongly altered rock rarely extends more than 15 m from the vein walls (Fig. 7a). Five alteration zones were defined: (1) adularia zone, (2) illite zone, (3) illite + smectite zone, (4) smectite zone, and (5) a late and overprinting kaolinite zone.

Unaltered samples of the crystal-rich rhyolitic ignimbrite (Páez et al., 2010) exhibit a high proportion of quartz, sanidine, plagioclase, biotite and amphibole crystal fragments surrounded by an ash-sized matrix made of deformed glass-shards. Fiamme structures up to several centimeters long are widespread in the rock, defining a eutaxitic texture with associated spherulitic textures developed inside the fiamme structures.

Petrography and standard X-ray diffraction treatment methods were used for clay mineral identification in 88 surface and drill-hole samples. Additionally, selected samples were studied with a JEOL JSM-6400 scanning electron microscope with a EDS detector coupled (Inca-xSight, Oxford Instruments) (SEM/EDS), at the Zaragoza University, Spain.

7.1. Adularia zone (adularia + albite + quartz + illite + pyrite)

This alteration zone is pale-gray in color and is characterized by its pervasive silicification. Primary pyroclastic textures are completely obliterated; quartz crystals are the only surviving primary mineral phase, but exhibit overgrowth textures; alkali feldspar, plagioclase and mafic minerals are completely replaced by an aggregate of quartz and adularia. The ignimbrite matrix is completely replaced by a polygonal mosaic of adularia, secondary quartz, illite, and variable amounts of albite (Fig. 7b). Pyrite is common as disseminations and is typically coarse-grained (usually between 5 and 7 vol.%). This alteration zone can be found only in the proximity of the ore shoots (Páez, 2012), and is commonly absent along low-grade and barren areas of the vein system.

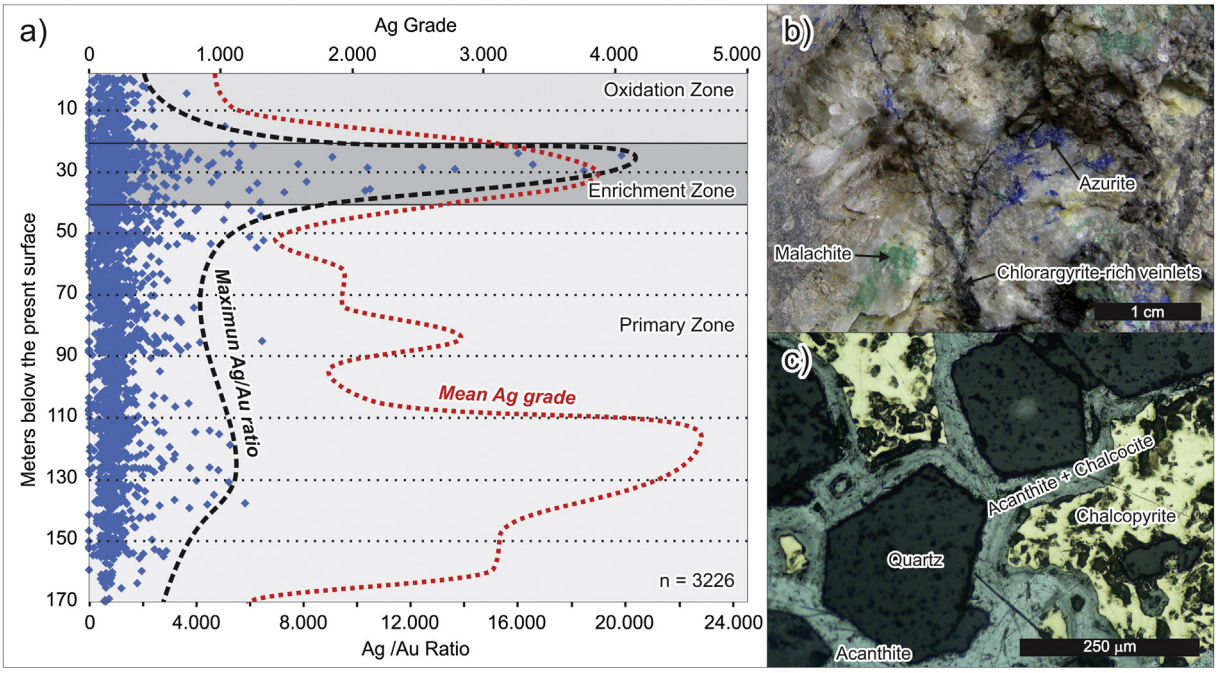

Fig. 6. a) Ag/Au versus depth profile showing the vertical extent of the oxidation, enrichment and primary ore zones of the Martha mine vein system. All available drill hole vein-assays were plotted (n = 9245). b) Secondary copper and silver minerals found as veinlets in the oxidation zone. c) Secondary acanthite and chalcocite partially replacing chalcopyrite crystals in the enrichment zone.

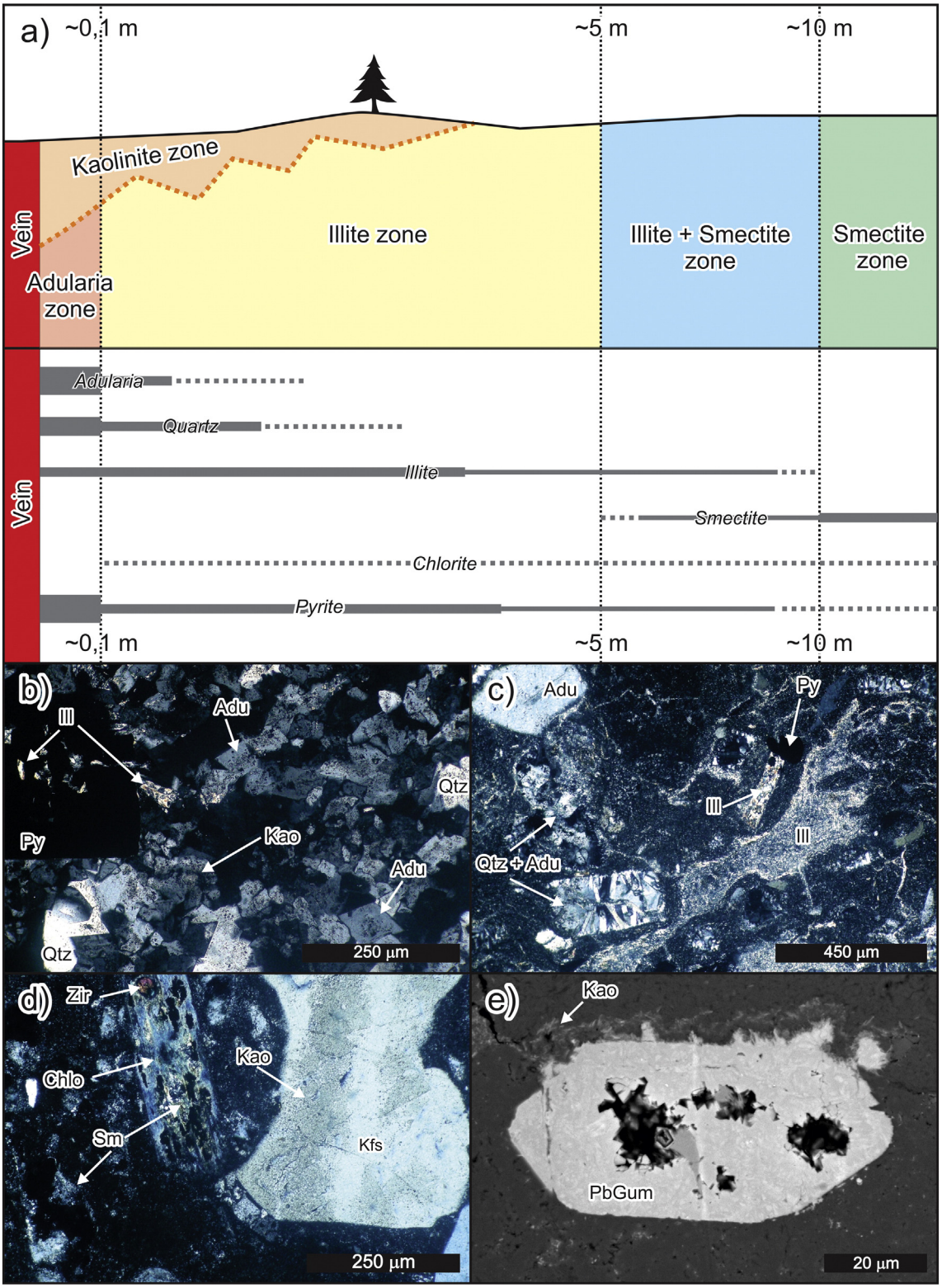

Fig. 7. a) Schematic cross section (not of scale) summarizing the distribution and abundance of alteration minerals around the veins at the Martha Mine. b) Adularia zone: ignimbrite matrix completely replaced by a polygonal mosaic of adularia, secondary quartz and illite. Kaolinite alteration can be recognized in the adularia crystal as an overprint. c) Illite zone: biotite crystal fragments and fiamme structures replaced by illite crystals, and alkali feldspar completely replaced by quartz and adularia. The ignimbrite matrix is completely replaced by fine-grained quartz and illite crystals. d) Smectite zone: biotite crystaloclast completely replaced by chlorite and smectite, smectite is also present in the ignimbrite matrix. On this particular sample a kaolinite overprinting can be recognized in the alkali feldspar crystals. e) Kaolinite zone: scanning electron microscope image showing plumbogummite and kaolinite crystals replacing part of the pyroclastic matrix ignimbrite. Abbreviations: Adu = adularia, Chlo = chlorite, Ill = illite, Kao = kaolinite, Kfs = alkali feldspar, PbGum = plumbogummite, Py = pyrite, Qtz = quartz, Sm = smectite, Zir = zircon.

7.2. Illite zone (illite + quartz + adularia ± albite ± chlorite ± pyrite)

This pale-gray to light-green alteration zone is characterized by weakly to moderately silicified rocks. Primary textures are commonly obliterated; however, further away from the vein walls some fiamme structures can still be identified on the rocks. Most crystal fragments are completely replaced (Fig. 7c), with the exception of quartz, which only shows minor overgrowths closer to the vein walls. Alkali feldspars are replaced by quartz + adularia or adularia + illite aggregates, whereas plagioclase crystals are commonly replaced by adularia + illite ± albite. Biotite is completely replaced by illite + adularia + opaque minerals ± chlorite. Ignimbrite matrix is always completely replaced by an aggregate of illite, secondary quartz and adularia; both the illite crystallinity and the content of quartz + adularia increase toward the vein walls. This alteration zone can be found right next to the adularia zone, or next to the vein walls around low grade or barren areas of the deposit.

7.3. Illite + smectite zone (illite + smectite ± adularia ± chlorite ± pyrite)

The illite zone grades laterally to less altered rocks with greenish colors. Silicification is commonly weak, and primary pyroclastic textures can be identified in some cases, especially in the outer regions of this alteration zone. Original feldspar and plagioclase crystals show partial alteration to an illite ± adularia association. Glass shards in the matrix and fiammes are replaced by illite + smectite, were the two clay minerals coexist without forming any interlayered structure. Secondary quartz, adularia and pyrite are commonly subordinated, and can be absent. Illite content decreases as smectite increases away from the vein walls.

7.4. Smectite zone (smectite ± chlorite ± pyrite)

This is the outer expression of the alteration halo, where primary textures are usually preserved. Most crystal fragments are largely unaltered; however, in some cases mafic minerals (mostly biotite) may be partially replaced by chlorite ± smectite ± opaque minerals (Fig. 7d). Glass shards in the matrix and most fiamme structures are altered to smectite. The intensity of this alterations decreases with increasing distance from the vein and is transitional to unaltered rocks.

7.5. Kaolinite zone (kaolinite + plumbogummite + jarosite)

This is a late and overprinting supergene alteration assemblage developed near the surface in close association with the mineralized structures. Hydrothermal adularia and alkali feldspars crystals are partially replaced by an fine-grained aggregate of low crystallinity kaolinite + plumbogummite (a lead-rich alunite group mineral $[PbAl_3(PO_4)_2(OH)_5 \cdot H_2O]$, Fig. 7e; Scott, 1990; Tzvetanova, 2003). Mafic minerals (mostly biotite) and hydrothermal pyrite are partially replaced by jarosite. Finally, the glass in the matrix and fiammes is replaced with a fine-grained aggregate of low crystallinity kaolinite + plumbogummite ± jarosite.

8. Fluid inclusion and stable isotopes

8.1. Fluid inclusion studies

Fluid inclusion studies where focused on primary inclusions (Shepherd et al., 1985; Bodnar et al., 1985; Wilkinson, 2001) found within quartz crystals from stages 3, 4, 5 and 6 mineralizing stages. Additionally, fluid inclusions analyzed by Rios et al. (2006) in pyrargyrite crystals, using NIR-SWIR light were also considered for stage 9.

Fluid inclusion studies were carried out at the Laboratorio de Inclusiones Fluidas y Metalogenesis (LIFM) of the Centro de Desenvolvimento da Tecnologia Nuclear (CDTN), Belo Horizonte, Brazil. Microscopy and microthermometric characterization of fluid inclusions were done using a Linkam FTIR-600 heating–freezing system stage attached to a modified Leica DMR-XP microscope (Rios et al., 2006). All determinations were photographed and recorded in video using a QICAM imaging system connected to a computer using Linkam Linksys 32 software. Primary fluid inclusions were selected and studied on the basis of their occurrence in growth zones and their morphology. Salinity values were calculated from the $T_{m(ice)}$ values using the method of Bodnar and Vityk (1994).

All analyzed samples contain two-phase (L + V) liquid-rich regular to ovoidal fluid inclusions, with filling (L:V) values between 75 and 90%, and size ranging from 4 μm to 30 μm. Obtained homogenization temperatures (T_h) range from 215.5 °C to 316.5 °C, and salinities from 0.5 to 3.5 wt.% NaCl eq., with the results summarized for each sample and mineralizing stage in Table 1 and in Fig. 8a. No clathrate formation was observed during these studies, suggesting a low CO_2 content, probably below 3.7 wt.% CO_2 (Hedenquist and Henley, 1985a).

When comparing the mean values of T_h and salinity from each mineralizing stage (Fig. 8a), two distinctive groups of fluid inclusions can be defined. The first group corresponds to a low salinity and high temperature cluster that includes stages 3, 4, 5 and 6; whereas the second one is a high salinity and low temperature group comprising stage 9 fluid inclusions. Moreover, T_h values decrease progressively within the first group (Fig. 8a), ranging from mean homogenization temperatures of 289.8 °C (stage 3) to 254.9 °C (stage 6).

8.2. Oxygen stable isotope study

Representative samples of quartz and adularia from several mineralizing stages (stages 1, 4, 5, 6 and 7) were selected for stable isotope determinations, which were performed at the Laboratorio de Isótopos Estables, of the Salamanca University, Spain (Table 2). Extracted gases were analyzed in a VG Isotech Micromass SIRA-II spectrometer, equipped with a cryogenic dispositive (cold finger). The measured isotopic ratios were reported in the conventional δ notation (‰). Oxygen extractions were performed by conventional methods (Clayton and Mayeda, 1963). The isotope ratios are given relative to the Standard Mean Ocean Water (SMOW) standard, with an analytical error of ±0.8‰ for $\delta^{18}O$.

Table 1
Summary information for samples used for fluid inclusion studies.

Sample ID	Vein	Sample type	Location	Mineralizing stage	Analyzed mineral	Salinity range (wt.% NaCl)	Th range (°C)	Number of measurements
P.Cata-A	Catalina	DDH sample	M-512 (188.5 m)	S3	Quartz	0.53–1.74	270.3–307.5	8
10688	R4	Hand specimen	Level 205	S4	Quartz	3.36–3.55	280.8–304.6	4
11321	Belén	DDH sample	M-360 (161.3 m)	S4	Quartz	2.24–2.41	266.8–277.6	2
P.Cata-B	Catalina	DDH sample	M-512 (188.5 m)	S4	Quartz	1.22–2.74	255.5–280.1	4
10689	R4	Hand specimen	Level 215	S5	Quartz	1.05–1.91	259.2–314.5	3
11301	Belén	DDH sample	M-259 (174.5 m)	S5	Quartz	1.4–1.91	239.5–316.5	4
11301 B	Belén	DDH sample	M-259 (174.5 m)	S5	Quartz	1.4–1.91	231.8–284.4	5
11324	Catalina	DDH sample	M-151 (51.5 m)	S6	Quartz	1.05–1.57	215.5–291.3	5
MM-9	Martha	Hand specimen	Level 290	S9	Pyrargirite	7.59–10.11	138–168	21 (Rios et al., 2006)

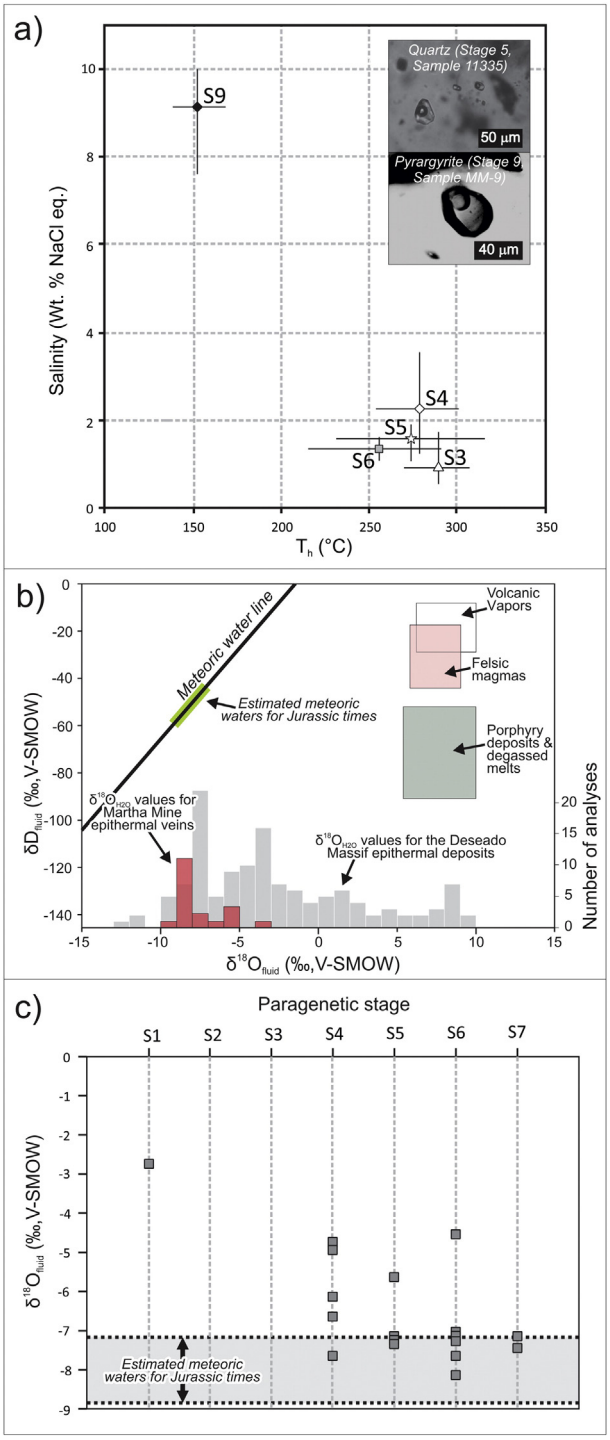

Fig. 8. a) Plot of homogenization temperature (T_h) versus salinity for fluids inclusions of Martha mine paragenetic stages 3, 4, 5, 6 and 9. b) Stable isotope (δD versus $\delta^{18}O$) plot showing the isotopic ratios of Jurassic meteoric waters for the Deseado Massif (Cravero et al., 1991), volcanic vapors, felsic magmas and porphyry ores (Hedenquist and Lowenstern, 1994; Taylor, 1986; Giggenbach, 1992), compared to $\delta^{18}O$ histograms of isotopic values of Martha mine (this work) and other Deseado Massif epithermal deposits (Schalamuk et al., 1997; Guido, 2002; Moreira, 2005; Permuy Vidal, 2014). c) Stable isotope ($\delta^{18}O$) values versus paragenetic stages, Jurassic meteoric waters for the Deseado Massif (Cravero et al., 1991) are shown for reference.

Obtained $\delta^{18}O_{H_2O}$ values range between −8.1‰ and −2.7‰ (Table 2 and Fig. 8b and c), and were recalculated from isotopic measurements following the fractionation equations of Zheng (1993), using the mean temperature of the fluid inclusion study (285 °C).

9. Geochronology

Sanidine (crystal-rich rhyolitic ignimbrite) and adularia (stage 6, Catalina Vein) step-heating ^{40}Ar–^{39}Ar gas release determinations were conducted at the National Geological Survey of Chile (SERNAGEOMIN) to constrain the timing of the hydrothermal activity and its temporal relation to their host rocks. Neutron-irradiation was performed at the nuclear reactor of the National Commission of Nuclear Energy, Chile (CChEN). For isotopic determination, samples were fused using a CO_2-laser system operating at a nominal output power of 30 W, and then analyzed in a MAP 215-50 mass spectrometer. Analytical conditions of the Ar–Ar system are described in more detail in Pérez de Arce et al. (2000, 2003).

Sanidine crystal fragments from the crystal-rich rhyolitic ignimbrite (sample 6627) yielded a plateau age of 157.6 Ma ± 1 Ma (Fig. 9a); this is a surface sample collected about 3 km to the west of the mine operations area, in order to avoid potential hydrothermal alteration of the mineralization host rocks.

Geochronological measurements on coarse-grained adularia crystals from stage 6 (sample 11329) yielded an age of 156.5 ± 0.9 Ma (Fig. 9b); this sample was collected from the underground workings of the Catalina Vein at the 170 level.

10. Discussion

Based on the paragenetic sequence, ore and gangue mineralogy, fluid inclusion data and stable isotopes information, the Martha mine vein system can be classified as an intermediate sulfidation epithermal deposit, with similar characteristics to those described by Hedenquist et al. (2000), Sillitoe and Hedenquist (2003) and Simmons et al. (2005) in several localities around the world, and also by Guido and Schalamuk (2003), Echavarría et al. (2005) and Fernández et al. (2008) in other areas of the Deseado Massif and Patagonia.

The complex paragenetic sequence of Ag–As–Sb sulfosalts and Cu–Pb–Zn sulfides, with the associated adularia-quartz-illite gangue (Fig. 3), can be simplified into three main evolutionary phases: a main hydrothermal phase, a late tectonic–hydrothermal phase and a post-mineral supergene phase.

10.1. Main hydrothermal phase

The main hydrothermal phase was developed as the infill of a series of vein structures with brecciated, massive, and minor crustiform to colloform textures (Figs. 3–5). The similarity and continuity of the hydrothermal infill on all the vein trends, and the absence of cross cutting relationships between them, suggests that all veins were formed during the evolution of the same hydrothermal system, as was previously proposed by Páez et al. (2011).

The paragenetic sequence of this phase is characterized by significant variations in the ore and gangue minerals contents (Fig. 3). As a general rule, base metal-bearing sulfides are better represented at early mineralizing stages (stages 2, 3 and 4), with their relative abundance progressively decreasing toward stage 4 (Fig. 3). On the other hand, silver-bearing sulfosalts increase in abundance from stage 2 to stage 4, and subsequently decrease in abundance from stage 4 to stage 5 (Fig. 3). Finally, these changes in ore mineralogy are also followed by an overall increase in abundance of adularia and quartz from stage 3 to stage 7 (Fig. 3). Mentioned changes in the mineralogy of the veins reflect an increase in the Ag/(Cu + Pb + Zn) ratio during the evolution of the vein system, occurring simultaneously with an overall decrease in the metal contents, as reflected by the overall decrease in the ore-bearing minerals in relation to the gangue minerals occurring from stage 2 to stage 7 (Fig. 3).

The hydrothermal alteration is zoned outward from the vein system, from the intense altered adularia zone, through the illite and illite-smectite zones, to the slightly altered smectite zone (Fig. 7a). The clay

Table 2
Summary information for samples used for oxygen isotope analyses.

Sample ID	Vein	Sample type	Location	Mineralizing stage	Mineral	$\delta^{18}O_{min}$ (‰)	$\delta^{18}O_{H_2O}$ (‰)
10657	R4	DDH sample	M-11 (77.1 m)	S1	Quartz	4.8	−2.75
10666	R4	DDH sample	M-472 (146.3 m)	S4	Adularia	−1.5	−6.14
P.Cata-B	Catalina	DDH sample	M-512 (188.5 m)	S4	Adularia	−0.1	−4.74
10666	R4	DDH sample	M-472 (146.3 m)	S4	Quartz	−0.1	−7.65
11331	Catalina	Hand specimen	Level 170	S4	Quartz	2.6	−4.95
P.Cata-B	Catalina	DDH sample	M-512 (188.5 m)	S4	Quartz	0.9	−6.65
11301	Belén	DDH sample	M-259 (174.5 m)	S5	Adularia	−1	−5.64
11301	Belén	DDH sample	M-259 (174.5 m)	S5	Quartz	0.3	−7.25
11311	Francisca	DDH sample	M-515 (65 m)	S5	Quartz	0.4	−7.15
11335	Catalina	Hand specimen	Level 200	S5	Quartz	0.2	−7.35
11317	Francisca	DDH sample	M-112 (79.4 m)	S6	Adularia	−2.4	−7.04
11317	Francisca	DDH sample	M-112 (79.4 m)	S6	Adularia	−2.5	−7.14
11329	Catalina	Hand specimen	Level 170	S6	Adularia	−2.5	−7.14
11302-A	Belén	DDH sample	M-223 (162 m)	S6	Adularia	−3.5	−8.14
11317	Francisca	DDH sample	M-112 (79.4 m)	S6	Quartz	−0.1	−7.65
11302-A	Belén	DDH sample	M-223 (162 m)	S6	Quartz	3	−4.55
11302-A	Belén	DDH sample	M-223 (162 m)	S6	Quartz	0.3	−7.25
11302-B	Belén	DDH sample	M-223 (162 m)	S7	Quartz	0.1	−7.45
11329-B	Catalina	Hand specimen	Level 170	S7	Quartz	0.4	−7.15

paragenesis of the alteration is in agreement with measured homogenization temperatures from stages 3 to 6 (Figs. 8a), suggesting temperatures higher than 220–250 °C close to the vein walls grading into temperatures below 150 °C away from the mineralized structures (Reyes, 1990; Simmons and Browne, 2000). The alteration mineral assemblage of quartz, adularia, albite, illite, smectite, chlorite and pyrite, indicate precipitation from a near-neutral to weakly alkaline chloride aqueous fluid, similar to those found in the main upwelling waters at active geothermal fields (Reyes, 1990; Simmons and Browne, 2000; Simmons et al., 2005). The overall CO_2 content of these chloride waters is interpreted to be low, as can be indirectly constrained from the absence of calcite in the alteration assemblage (Hedenquist and Browne, 1989; Simmons and Browne, 2000; Simpson and Mauk, 2007), and also due to the lack of clathrate formation during the fluid inclusion studies (Hedenquist and Henley, 1985a).

Fluid inclusion data also shows that hydrothermal fluids were low salinity chloride aqueous solutions (0.5 to 3.5 wt.% NaCl eq.) that evolved following a progressive cooling pattern from about 290 °C in stage 3, to around 255 °C in stage 6 (Figs. 8a), including a slight salinity peak associated to stage 4 (with mean salinity = 2.25 wt.% NaCl).

Obtained $\delta^{18}O_{H_2O}$ values show a strong correlation between the isotopic values of Jurassic meteoric waters in the Deseado Massif, determined by Cravero et al. (1991), and the obtained $\delta^{18}O_{H_2O}$ values of Martha mine veins (Fig. 8b), implying a high proportion of meteoric waters at the hydrothermal fluids responsible of the ore deposition of stages 1, 4, 5, 6 and 7. However, a small magmatic component can be interpreted as some of the $\delta^{18}O_{H_2O}$ values are higher than the reference isotopic values determined for the Jurassic meteoric waters (Cravero et al., 1991; Hedenquist and Lowenstern, 1994; Taylor, 1986; Giggenbach, 1992), especially considering isotopic values of stages 1 and 4 (Fig. 8c).

Finally, geochronological measurements on coarse-grained adularia crystals from stage 6 yielded an age of 156.5 ± 0.9 Ma (Fig. 9b), constrain the hydrothermal activity into Upper Jurassic (Kimmeridgian) times (Cohen et al., 2013). This age is comparable to similar values determined for the volcanic activity of the Primero de Abril Caldera (156.9 ± 0.7 Ma; Ruiz, 2012), suggesting a possible relationship between the Martha mine hydrothermal system and the waning stages of the caldera volcanism (late to post-caldera stage) whose approximate edge is located 1–3 km to the north of the vein system (Páez et al., 2010). The obtained sanidine age for the crystal-rich rhyolitic ignimbrite (157.6 Ma ± 1 Ma, Fig. 9a) shows this unit as clearly pre-mineral in nature, and also as a pre-caldera volcanic deposit in the model of Ruiz (2012). Both obtained ages are in agreement with other regional Ar–Ar and U–Pb geochronological studies performed by Féraud et al. (1999), Echeveste (2005), Wallier (2009) and Ruiz (2012) on the southwestern portion of the Deseado Massif.

10.2. Ore deposition mechanisms during the main hydrothermal phase

Boiling, mixing and/or cooling of the hydrothermal solutions are considered the main mechanisms controlling ore deposition in shallow epithermal environments (e.g., Hedenquist et al., 2000; Simmons et al., 2005; Leach and Corbett, 2008). Among these three, most researchers recognize boiling as the main process affecting the pH, fluid composition and mineral solubility in the hydrothermal solutions, and therefore

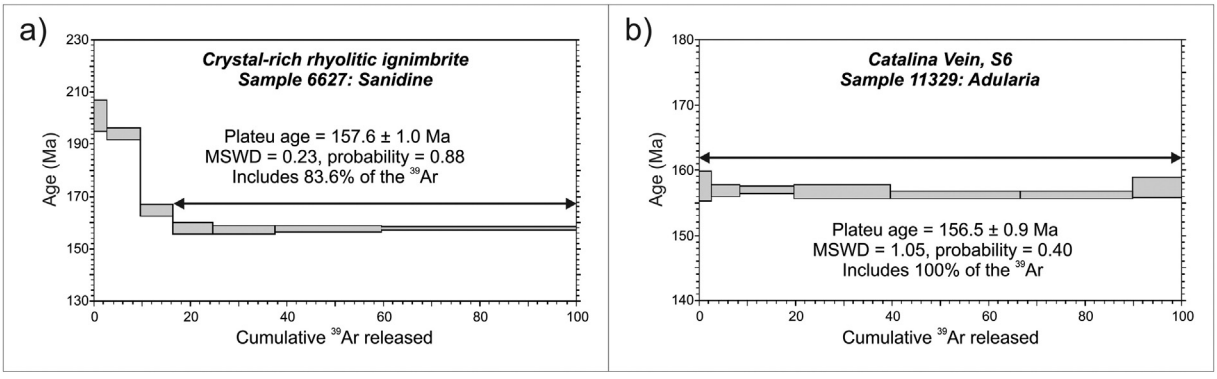

Fig. 9. Laser ^{40}Ar–^{39}Ar age determinations for the Martha mine veins and host rocks. a) Sanidine crystal fragments from the crystal-rich rhyolitic ignimbrite (Sample Id: 6627, surface outcrop sample). b) Adularia crystals from stage 6 at Catalina vein (Sample Id: 11329, underground workings at 170 level).

controlling ore deposition (e.g., Skinner, 1997; Simmons et al., 2005; Canet et al., 2011; Moncada et al., 2012). Boiling is also the most cited ore-controlling process in the low- to intermediate-sulfidation epithermal veins from the Deseado Massif (e.g., Cerro Vanguardia Mine, Manantial Espejo Mine, Cerro Negro Project, La Josefina Project; see Schalamuk et al., 2005; Echavarría et al., 2005; Wallier, 2009; Permuy Vidal, 2014; Moreira and Fernández, 2014).

Mineralogical and fluid inclusion evidence of a boiling system includes ore-bearing colloform-banded textures with amorphous silica, platy calcite (commonly later replaced by quartz), adularia, and coexisting liquid-rich and vapor-rich fluid inclusions, among others (Hedenquist et al., 2000; Simmons et al., 2005; Leach and Corbett, 2008). Except for the presence of widespread adularia across most of the paragenetic scheme (stages 3 to 7, Fig. 3), veins at the Martha mine lacks most of these features, suggesting non-boiling conditions for mineral deposition during the main hydrothermal phase. Relatively constant fluid inclusion liquid-to-vapor ratios were observed among samples from different mine levels, and across all stages of mineralization (L:V variations below 15%), which also is one line of evidence for a non-boiling system. Additionally, the absence of more indirect evidence of boiling, such as hydrothermal eruption breccias, and/or extensive steam-heated alteration zones capping the epithermal veins, also points for a non-boiling system (Hedenquist and Henley, 1985b; Hedenquist et al., 2000).

Considering the progressive cooling pattern evidenced by fluid inclusions from stages 3 to 6 (Fig. 8a), and the overall decrease in $\delta^{18}O_{H_2O}$ values from stages 1 to 7 (Fig. 8c), cooling of the hydrothermal solutions along with dilution by "fresh" deep-circulating non-saline (i.e., meteoric) waters, fits with the results of the analyses and observations. Dilution by a cooler meteoric component is also consistent with the overall decrease in ore-bearing mineral contents with increasing time (Fig. 3), as more diluted solutions would have been responsible for mineral deposition of each successive mineralizing stage.

Cooling and dilution involving different types of meteoric-dominant waters (e.g., deep-circulating ground waters, shallow oxygenated ground waters, bicarbonate waters and low pH acid sulfate waters; see Leach and Corbett, 2008) have been reported as an important ore-controlling process in epithermal deposits such as Veta Madre (Mexico, Mango et al., 2014), Buckskin Mountain (USA, Vikre, 2007), Creede district (USA, Plumlee, 1994), Tayoltita (Mexico, Conrad et al., 1992), and several other low-sulfidation epithermal deposits around the world (Hedenquist and Lowenstern, 1994; Hedenquist et al., 2000; Simmons et al., 2005; Leach and Corbett, 2008), however this represents the first mention of these processes for any epithermal deposit at the Deseado Massif.

10.3. Late tectonic–hydrothermal phase

After the main hydrothermal event, irregularly-shaped bodies of massive fault breccias and foliated cataclasites (Passchier and Trouw, 2005) developed in response to the tectonic reactivation of the Martha–R4 vein trend, defining a late-stage tectonic–hydrothermal phase for the evolution of the Martha mine vein system (Stage 8, Fig. 3). These cemented breccias are the result of the deposition of minerals from circulating fluids in synchronism with the deformation (Passchier and Trouw, 2005); in the case of Martha mine those minerals are mostly silica-group minerals, especially chalcedony (Fig. 3).

As these breccia bodies cross cut the previously deposited mineralization (Figs. 3 and 5), the presence of circulating fluids resulted in the mechanical and chemical remobilization of the silver-rich sulfosalts (e.g., Gilligan and Marshall, 1987; Marshall and Gilligan, 1987; Hobbs, 1987; Gu et al., 2007). Mechanical remobilization (Marshall and Gilligan, 1987) occurred along with fragile deformation, and is evidenced by the presence of cataclastically deformed angular-shaped sulfide clasts within the breccias and cataclasites, and also by the presence of mechanically concentrated sulfide grains within the foliation planes of the cataclasites. Chemical remobilization occurs through dissolution and re-precipitation of previously deposited ore-minerals in response of fluid circulation in close relationship with the deformation (Marshall and Gilligan, 1987). At Martha Mine, this is evidenced by the spatial association observed between the high-grade stage 8 breccias and the high-grade hydrothermal mineralization (stages 2 to 6), and by the association of barren stage 8 breccias to the barren mineralizing stages (stages 6 and 7) or the host-rock. Additional evidence supporting this idea is the presence of a new generation of sulfides, especially pyrite and chalcopyrite, overgrowing and healing fractures over cataclastically deformed sulfides in stage 8 breccias. Finally, these ideas are also supported by the depositional textures of some of the stage 8 and stage 9 sulfosalts, developed as cavity infill in stage 8 or small veinlets in stage 9 (Fig. 5), which suggest their precipitation from hydrothermal solutions.

Based on the fluid inclusions measured in stage 9, the fluids circulating in synchronism with the deformation are interpreted to be aqueous solutions of lower temperatures and higher salinities than those of the main hydrothermal phase (Figs. 8a). Measured homogenization temperatures show a mean temperature of 152.9 °C, which seem to continue the overall cooling pattern identified in the main hydrothermal phase (Figs. 8a). In contrast, salinities measured show significantly higher values during this phase, ranging between 7.7 and 9.9 wt.% NaCl eq. (Figs. 8a). These higher salinities are difficult to interpret based on the available data, however it possible to speculate on a small magmatic input occurring along with deformation, as there is no pre-Jurassic marine or evaporitic rocks that can be the source of these high salinity fluids in the Deseado Massif.

Constraining the age of these processes is complicated as there are no datable mineral phases to analyze. However, Páez et al. (2011) identified a series of post-mineral fault systems that crosscut and displace both the hydrothermal veins and tectonic–hydrothermal breccias, and interpreted them to be post-Kimmeridgian to pre-Aptian in age (i.e., between 152 and 113 Ma). This age constraint supports the interpreted continuation of the overall cooling pattern identified in the main hydrothermal phase, and allows speculating that the tectonic–hydrothermal phase was developed during tectonic reactivations occurring in the waning stages of the main hydrothermal system, and therefore they are also Late Jurassic in age.

10.4. Post-mineral supergene phase

The shallow portions of the vein system are characterized by a series of post-mineral vertical changes in both geochemistry and mineralogy, allowing the definition of a 40–50 m thick zone with evidences for dissolution and re-precipitation of silver and copper minerals due to the extensive weathering of the mineralized bodies (Fig. 6a).

The presence of Fe and Pb sulfates, Cu and Pb carbonates and Ag, Cu and Pb chlorides in the upper portions of the mineralized structures (Fig. 6b), along with jarosite, kaolinite and alunite group minerals (plumbogummite) in the host rocks (Fig. 7a), suggests that acidic and oxidizing conditions prevailed in the upper 20 m of the deposit due to the destruction of the ore-sulfides by the circulation of descending cold (<40 °C) meteoric waters, dissolving and mobilizing Ag and Cu from their hosting minerals (Scott, 1990; Sillitoe and McKee, 1996; Hartley and Rice, 2005). Below this supergene zone, the presence of Cu and Ag sulfides and sulfosalts with replacement textures over primary ore minerals (Fig. 6c), indicate the presence of a 20–30 m thick secondary enriched zone developed where reduced conditions prevailed, leading to the precipitation of the previously mobilized metals from the descending meteoric waters (Scott, 1990; Sillitoe and McKee, 1996; Greffié et al., 2002; Hartley and Rice, 2005).

These changes are the youngest evidence of a post-mineral modification occurring to the Martha mine vein system, and its close association to the current topography suggests a Pleistocene to Holocene age for these mineralogical changes.

11. Conclusions

Martha mine is an intermediate sulfidation epithermal system characterized by a strong structural control on its grade distribution. Within single veins (Fig. 2b), mineralization is represented as broad areas defining gently plunging first order ore-shoots resulting from the combination of several high grade second order ore-shoots, which can be individually associated with dilatational jogs and step-overs (Páez et al., 2011). Within this structural environment, mineralization evolved through three main phases, which can be defined based on the processes operating during its formation: a main hydrothermal phase, a late tectonic–hydrothermal phase and a post-mineral supergene phase.

The main hydrothermal phase was the result of mineral deposition due to cooling and dilution of low salinity hydrothermal solutions with isotopic compositions resembling high proportions of meteoric waters. These physicochemical conditions combined with an efficient network of structural conduits (vein intersections, jogs and step-over zones), provided the necessary conditions for the construction of the high grade second order ore-shoots that characterize the Martha mine epithermal vein system, which are the result of the focusing and concentration of the ascending hydrothermal solutions. The overlapping of these small-sized ore-shoots led to the development of the first order ore-shoots.

Afterwards, the late tectonic–hydrothermal phase occurred through the development of irregularly-shaped bodies of fault breccias and cataclasites related to tectonic reactivations of the Martha–R4 vein trend during the waning stages of the hydrothermal system. The interplay between deformation and fluid circulation resulted in mechanical and chemical remobilization of the previously deposited silver-rich sulfosalts. This late tectonic–hydrothermal phase strongly contributes to increase the grades along the Martha–R4 vein trend, and therefore is considered an essential process in order to build the highest-grade portions of the ore-shoots developed along the Martha–R4 vein trend.

Finally, the post-mineral supergene phase was responsible for the generation of a 40-50 m thick zone with evidence of weathering of the mineralized bodies in response to the circulation of descending cold (<40 °C) meteoric waters. These changes defined a 20 m thick oxidized zone close to the surface, followed by a 20–30 m thick secondary enrichment zone below it. Despite its small size and vertical extension, the secondary enrichment level at Martha mine constitutes an important economic factor for the mining operations as it helped to increase the silver grades in the shallower portion of the vein system.

Martha mine constitutes an exceptional example of the interplay of a series of hydrothermal (mostly physicochemical), structural and supergene processes in order to form high grade "bonanza" ore-shoots in the epithermal environment, and show that relatively small deposits can show very high grades if the required conditions occurred during the circulation of the hydrothermal solutions.

Acknowledgments

This work is part of a PhD thesis carried out at the Universidad Nacional de La Plata (UNLP) with the support of Coeur d'Alene Mines and the 2008 Hugh E. McKinstry Student Research Award from the Society of Economic Geologists. The authors wish to thank Alfredo Cruzat, Claudio Romo and the Martha mine staff for their help, discussions and access to data. Also we would like to thank Conrado Permuy Vidal, Sebastian Jovic and Luciano Lopez for the constant support and constructive comments on early versions of this manuscript. Last but not the least, the authors wish to thank the thoughtful revisions made by Editor-in-chief Franco Pirajno and two anonymous reviewers which significantly improved this manuscript.

References

Arribas Jr., A., Schalamuk, I.B., de Barrio, R., Fernández, R., Itaya, T., 1996. Edades Radimétricas de Mineralizaciones Epitermales Auríferas del Macizo del Deseado, Provincia de Santa Cruz, Argentina. IGCP Project 342: Age and isotopes of South American Ores. XXXIX Congresso Brasileiro de Geología, pp. 254–257.

Berger, B.R., Tingley, J.V., Drew, L.J., 2003. Structural localization and origin of compartmentalized fluid flow, Comstock Lode, Virginia City, Nevada. Econ. Geol. 98, 387–408.

Bodnar, R.J., Vityk, M.O., 1994. Interpretation of microthermometric data for H_2O–NaCl fluid inclusions. In: De Vivo, B., Frezzotti, M.L. (Eds.), Fluid Inclusions in Minerals: Methods and Applications. Published by Virginia Tech, Blacksburg, VA, pp. 117–130.

Bodnar, R.J., Reynolds, T.J., Kuehn, C.A., 1985. Fluid inclusion systematics in epithermal systems. Geology and geochemistry of epithermal systems. In: Berger, B.R., Bethke, P.M. (Eds.), Reviews in Economic Geology 2, pp. 73–97.

Canet, C., Franco, S.I., Prol-Ledesma, R.M., González-Partida, E., Villanueva-Estrada, R.E., 2011. A model of boiling for fluid inclusion studies: application to the Bolaños Ag–Au–Pb–Zn epithermal deposit, Western Mexico. J. Geochem. Explor. 110, 118–125.

Clayton, R., Mayeda, T., 1963. The use of bromine pentafluoride in the extraction of oxygen from oxides and silicates for isotopic analysis. Geochim. Cosmochim. Acta 27, 43–52.

Cohen, K.M., Finney, S.C., Gibbard, P.L., Fan, J.X., 2013. The ICS International Chronostratigraphic Chart. Episodes 36, 199–204.

Conrad, M.E., Petersen, U., Neil, R.O., 1992. Evolution of an Au–Ag-producing hydrothermal system: the Tayoltita Mine, Durango, Mexico. Econ. Geol. 87, 1451–1474.

Cox, S.F., 2005. Coupling between deformation, fluid pressures and fluid flow in ore producing hydrothermal systems at depth in the crust. Economic Geology 100th Anniversary Volumepp. 1–35.

Cravero, F., Domínguez, E., Murray, H.H., 1991. Valores de $\delta^{18}O$ y δD en caolinitas indicadoras de un clima templado-húmedo para el Jurásico Superior-Cretácico Inferior de la Patagonia. Rev. Asoc. Geol. Argent. 46, 20–25.

Dong, G., Morrison, G.W., 1995. Adularia in epithermal veins, Queensland: morphology, structural state and origin. Mineral. Deposita 30, 11–19.

Echavarría, L.E., Schalamuk, I., Etcheverry, R.O., 2005. Geologic and tectonic setting of Deseado Massif epithermal deposits, Argentina, based on El Dorado-Monserrat. J. S. Am. Earth Sci. 19, 415–432.

Echeveste, H., 2005. Metalogénesis del Distrito Argento-Aurífero Manantial Espejo, Macizo del Deseado. Provincia de Santa Cruz PhD thesis, Universidad Nacional de La Plata, La Plata, Argentina (272 pp.).

Echeveste, H., Fernández, R., Bellieni, G., Tessone, M., Llambías, E., Schalamuk, I., Piccirillo, E.M., De Min, A., 2001. Relaciones entre las Formaciones Bajo Pobre y Chon Aike (Jurásico Medio a Superior) en el área Estancia El Fénix-Cerro Huemul, zona centro-occidental del Macizo del Deseado, provincia de Santa Cruz. Rev. Asoc. Geol. Argent. 56, 548–558.

Féraud, G., Alric, V., Fornari, M., Bertrand, H., Haller, M.J., 1999. $^{40}Ar/^{39}Ar$ dating of the Jurassic volcanic province of Patagonia: migrating magmatism related to Gondwana break-up and subduction. Earth Planet. Sci. Lett. 172, 83–96.

Fernández, R., Blesa, A.P., Moreira, P., Echeveste, H., Mykietiuk, K., De Palomera, P.A., Tessone, M., 2008. Los depósitos de oro y plata vinculados al magmatismo jurásico de la Patagonia: revisión y perspectivas para la exploración. Rev. Asoc. Geol. Argent. 63, 665–681.

Feruglio, E., 1949. Descripción geológica de la Patagonia 3 Volumes Dirección Nacional de Yacimientos Petrolíferos Fiscales, Buenos Aires.

Giacosa, R., Zubia, M.A., Sánchez, M., Allard, J., 2010. Meso-Cenozoic tectonics of the southern Patagonian foreland: structural evolution and implications for Au–Ag veins in the eastern Deseado Region (Santa Cruz, Argentina). J. S. Am. Earth Sci. 30, 134–150.

Giggenbach, W.F., 1992. Magma degassing and mineral deposition in hydrothermal systems along convergent plate boundaries. Econ. Geol. 87, 1927–1944.

Gilligan, L., Marshall, B., 1987. Textural evidence for remobilization in metamorphic environments. Ore Geol. Rev. 2, 205–229.

González Guillot, M., De Barrio, R.E., Ganem, F., 2004. Mina Martha, un yacimiento epitermal argentifero en el Macizo del Deseado, Provincia de Santa Cruz. VII Congreso De Mineralogía y Metalogenia, pp. 199–204.

Greffié, C., Bailly, L., Milési, J.P., 2002. Supergene alteration of primary ore assemblages from low-sulfidation Au–Ag epithermal deposits at Pongkor, Indonesia, and Nazareño, Perú. Econ. Geol. 97, 561–571.

Gu, L., Zheng, Y., Tang, X., Zaw, K., Della-pasque, F., Wu, C., Tian, Z., Lu, J., Ni, P., Li, X., Yang, F., Wang, X., 2007. Copper, gold and silver enrichment in ore mylonites within massive sulphide orebodies at Hongtoushan VHMS deposit, N.E. China. Ore Geol. Rev. 30, 1–29.

Guido, D., 2002. Geología y metalogénesis del sector oriental del Macizo del Deseado, provincia de Santa Cruz PhD thesis, Universidad Nacional de La Plata, La Plata, Argentina (226 pp., Available at: http://sedici.unlp.edu.ar/handle/10915/4617).

Guido, D., 2004. Subdivisión litofacial e interpretación del volcanismo jurásico (Grupo Bahía Laura) en el este del Macizo del Deseado, provincia de Santa Cruz. Rev. Asoc. Geol. Argent. 59, 727–742.

Guido, D., 2005. Estudio comparativo de mineralizaciones epitermales en el este del Macizo del Deseado. XVI Congreso Geológico Argentino. Asociación Geológica Argentina, La Plata, Argentina, CD-ROM.

Guido, D., Campbell, K., 2011. Jurassic hot spring deposits of the Deseado Massif (Patagonia, Argentina): characteristics and controls on regional distribution. J. Volcanol. Geotherm. Res. 203, 35–47.

Guido, D., Schalamuk, I., 2003. Genesis and exploration potential for low sulfidation epithermal deposits in the Deseado Massif, Argentinean Patagonia. In: Eliopoulos, D.G. (Ed.), Mineral Exploration and Sustainable Development. Society for Geology Applied to Mineral Deposits, Athens, Greece, pp. 493–496.

Guido, D., Escayola, M.P., De Barrio, R.E., 2006. La Formación Bajo Pobre (Jurásico) en el este del Macizo del Deseado, Patagonia: vinculación con el Grupo Bahía Laura. Rev. Asoc. Geol. Argent. 61, 187–196.

Hartley, A.J., Rice, C.M., 2005. Controls on supergene enrichment of porphyry copper deposits in the Central Andes: a review and discussion. Mineral. Deposita 40, 515–525.
Hedenquist, J.W., Browne, P.R., 1989. The evolution of the Waiotapu geothermal system, New Zealand, based on the chemical and isotopic composition of its fluids, minerals and rocks. Geochim. Cosmochim. Acta 53, 2235–2257.
Hedenquist, J., Henley, R., 1985a. The importance of CO_2 on freezing point measurements of fluid inclusions: evidence from active geothermal systems and implications for epithermal ore deposition. Econ. Geol. 80, 1379–1406.
Hedenquist, J., Henley, R., 1985b. Hydrothermal eruptions in the Waiotapu geothermal system, New Zealand; their origin, associated breccias, and relation to precious metal mineralization. Econ. Geol. 80, 1640–1668.
Hedenquist, J.W., Lowenstern, J.B., 1994. The role of magmas in the formation of hydrothermal ore deposits. Nature 370, 519–527.
Hedenquist, J., Arribas, A., Gonzalez-Urien, E., 2000. Exploration for epithermal gold deposits. In: Hagemann, S.G., Brown, P.E. (Eds.), Reviews in Economic Geology Number 13: Gold in 2000. Society of Economic Geologists, pp. 245–277.
Hobbs, B., 1987. Principles involved in mobilization and remobilization. Ore Geol. Rev. 2, 37–45.
Jovic, S.M., Guido, D.M., Schalamuk, I.B., Ríos, F.J., Tassinari, C.C.G., Recio, C., 2011. Pingüino In-bearing polymetallic vein deposit, Deseado Massif, Patagonia, Argentina: characteristics of mineralization and ore-forming fluids. Mineral. Deposita 46, 257–271.
Leach, T., Corbett, G., 2008. Fluid mixing as a mechanism for bonanza grade epithermal gold formation. Terry Leach Symposium 2008 (12 pp. Available at: http://corbettgeology.com/).
Mango, H., Arehart, G., Oreskes, N., Zantop, H., 2014. Origin of epithermal Ag–Au–Cu–Pb–Zn mineralization in Guanajuato, Mexico. Mineral. Deposita 49, 119–143.
Márquez-Zavalía, M.F., Bindi, L., Márquez, M., Menchetti, S., 2008. Se-bearing polybasite-Tac from the Martha mine, Macizo del Deseado, Santa Cruz, Argentina. Mineral. Petrol. 94, 145–150.
Marshall, B., Gilligan, L., 1987. An introduction to remobilization: information from orebody geometry and experimental considerations. Ore Geol. Rev. 2, 87–131.
Micklethwaite, S., 2009. Mechanisms of faulting and permeability enhancement during epithermal mineralisation: Cracow goldfield, Australia. J. Struct. Geol. 31, 288–300.
Moncada, D., Mutchler, S., Nieto, A., Reynolds, T.J., Rimstidt, J.D., Bodnar, R.J., 2012. Mineral textures and fluid inclusion petrography of the epithermal Ag–Au deposits at Guanajuato, Mexico: application to exploration. J. Geochem. Explor. 114, 20–35.
Moreira, P., 2005. Geología y metalogénesis del distrito La Josefina, macizo del Deseado, provincia de Santa Cruz PhD thesis, Universidad Nacional de La Plata, La Plata, Argentina (360 pp. Available at: http://sedici.unlp.edu.ar/handle/10915/4478).
Moreira, P., Fernández, R.R., 2014. La Josefina Au–Ag deposit (Patagonia, Argentina): a Jurassic epithermal deposit formed in a hot spring environment. Ore Geol. Rev. 67, 297–313.
Morrison, G.W., Dong, G., Jaireth, S., 1995. Textural Zoning in Epithermal Quartz Veins in Queensland Field Guide. James Cook University of North Queensland, Townsville, p. 25 (AMIRA project P247).
Páez, G.N., 2012. Génesis del yacimiento de metales preciosos Mina Martha, sector sudoccidental del Macizo del Deseado, provincia de Santa Cruz PhD thesis, Universidad Nacional de La Plata, La Plata, Argentina (241 pp. Available at: http://sedici.unlp.edu.ar/handle/10915/25765).
Páez, G.N., Ruiz, R., Guido, D.M., Jovic, S.M., Schalamuk, I., 2010. Estratigrafía volcánica del yacimiento argentífero Mina Martha, Macizo del Deseado, Provincia de Santa Cruz. Rev. Asoc. Geol. Argent. 67, 77–90.
Páez, G.N., Ruiz, R., Guido, D., Jovic, S., Schalamuk, I., 2011. Structurally controlled fluid flow: high-grade silver ore-shoots at Martha epithermal mine, Deseado Massif, Argentina. J. Struct. Geol. 33, 985–999.
Pankhurst, R.J., Leat, P.T., Sruoga, P., Rapela, C.W., Márquez, M., Storey, B.C., Riley, T.R., 1998. The Chon Aike province of Patagonia and related rocks in West Antarctica: a silicic large igneous province. J. Volcanol. Geotherm. Res. 81, 113–136.
Pankhurst, R., Riley, T., Fanning, C., Kelley, S., 2000. Episodic silicic volcanism in Patagonia and the Antarctic Peninsula: chronology of magmatism associated with the break-up of Gondwana. J. Petrol. 41, 605–625.
Panza, J.L., Haller, M.J., 2002. El volcanismo jurásico. In: Haller, M.J. (Ed.), Geología y recursos Naturales de Santa Cruz. Relatorio del XV Congreso Geológico Argentino, pp. 89–102.
Passchier, C.W., Trouw, R.A.J., 2005. Micro-tectonics. 2nd edition. Springer, Berlin (366 pp.).
Pérez de Arce, C., Becker, T., Roeschmann, C., 2000. El nuevo sistema de datación $^{40}Ar/^{39}Ar$ equipado con láser de CO_2 en el SERNAGEOMIN. IX Congreso Geológico Chileno 1, p. 675.
Pérez de Arce, C., Matthews, S., Klein, J., 2003. Geochronology by the $^{40}Ar/^{39}Ar$ method at the SERNAGEOMIN Laboratory, Santiago, Chile. International Conference on Research Reactor, Utilization, Safety, Decommissioning, Fuel and Waste Management, Actas. Santiago, Chile, pp. 82–83.
Permuy Vidal, C., 2014. Caracterización detallada de la mineralización en veta Eureka, y su comparación con otras mineralizaciones del Distrito Cerro Negro, Macizo del Deseado, Santa Cruz, Argentina PhD thesis, Universidad Nacional de La Plata, La Plata, Argentina (275 pp. Available at: http://sedici.unlp.edu.ar/handle/10915/36121).
Plumlee, G., 1994. Fluid chemistry evolution and mineral deposition in the Creede epithermal system. Econ. Geol. 89, 1860–1882.
Reyes, A., 1990. Petrology of Philippine geothermal systems and the application of alteration mineralogy to their assessment. J. Volcanol. Geotherm. Res. 43, 279–309.
Rios, F.J., Alves, J.V., Pérez, C.A., Costa, É.C., Rosière, C.A., Fuzikawa, K., Correia Neves, J.M., Chaves, A. de O., Prates, S.P., de Barrio, R.E., 2006. Combined investigations of fluid inclusions in opaque ore minerals by NIR/SWIR microscopy and microthermometry and synchrotron radiation X-ray fluorescence. Appl. Geochem. 21, 813–819.
Ruiz, R., 2012. Geología y Mineralizaciones del sector sudoccidental del Macizo del Deseado, Santa Cruz PhD thesis, Universidad Nacional de La Plata, La Plata, Argentina (314 pp. Available at: http://sedici.unlp.edu.ar/handle/10915/25786).
Ruiz, R., Páez, G.N., Guido, D.M., Schalamuk, I.B., 2008a. Ambiente Volcánico y Mineralizaciones del Área Cerro 1ro de Abril, Sector Sudoccidental del Macizo del Deseado, Santa Cruz, Argentina. XVII Congreso Geológico Argentino. Actas (II). Jujuy, Argentina, pp. 897–898.
Ruiz, R., Páez, G.N., Guido, D.M., Schalamuk, I.B., 2008b. Extensas Manifestaciones de Hot Spring Asociadas al Centro Volcánico Jurásico del Área Cerro 1ro de Abril, Sector Sudoccidental del Macizo del Deseado, Santa Cruz, Argentina. XVII Congreso Geológico Argentino. Actas (II). Jujuy, Argentina, pp. 895–896.
Schalamuk, I., Zubia, M.A., Genini, A., Fernández, R., 1997. Jurassic epithermal Au–Ag deposits of Patagonia, Argentina. Ore Geol. Rev. 12, 173–186.
Schalamuk, I., De Barrio, R.E., Zubia, M.A., Genini, A., Echeveste, H., 1999. Provincia Auroargentífera del Deseado, Santa Cruz. In: Zappettini, E.O. (Ed.), Recursos Minerales De La República Argentina. Instituto de Geología y Recursos Minerales, SEGEMAR, Buenos Aires, Argentina, pp. 1177–1188.
Schalamuk, I., Ríos, F.J., de Barrio, R.E., Moreira, P., Echeveste, H., Cunnigham, C., Alves, J.V., 2005. Mineralized fluids related to Ag–Au ores in selected districts of epithermal province Macizo del Deseado, Southern Patagonia, Argentina. XVI Congreso Geológico Argentino, Proceedings CD-ROM.
Scott, K.M., 1990. Origin of alunite- and jarosite-group minerals in the Mt. Leyshon epithermal gold deposit, northeast Queensland, Australia. Am. Mineral. 75, 1176–1181.
Shepherd, T.J., Ranbin, A.H., Alderton, D.H.M., 1985. A Practical Guide to Fluid Inclusion Studies. Blackie, Glasgow (239 pp.).
Sillitoe, R., Hedenquist, J., 2003. Linkages between volcanotectonic settings, ore-fluid compositions, and epithermal precious metal deposits. In: Simmons, S., Graham, I. (Eds.), Special Publication No. 10: Volcanic, Geothermal, and Ore-Forming Fluids: Rulers and Witnesses of Processes within the Earth. Society of Economic Geologists, Littleton, CO, pp. 315–343.
Sillitoe, R.H., McKee, E.H., 1996. Age of supergene oxidation and enrichment in the Chilean porphyry copper province. Econ. Geol. 91, 164–179.
Simmons, S.F., Brown, K.L., 2006. Gold in magmatic hydrothermal solutions and the rapid formation of a giant ore deposit. Science 314, 288–291.
Simmons, S., Browne, P.R.L., 2000. Hydrothermal minerals and precious metals in the Broadlands–Ohaaki geothermal system: implications for understanding low-sulfidation epithermal environments. Econ. Geol. 95, 971–999.
Simmons, S., White, N.C., John, D.A., 2005. Geological characteristics of epithermal precious and base metal deposits. Economic Geology, 100th Anniversary Volume. Society of Economic Geologists, pp. 485–522.
Simpson, M., Mauk, J.L., 2007. The Favona Epithermal Gold–Silver Deposit, Waihi, New Zealand. Econ. Geol. 102, 817–839.
Skinner, B.J., 1997. Hydrothermal mineral deposits: what we do and don't know. In: Barnes, H.L. (Ed.), Geochemistry of Hydrothermal Ore Deposits, third ed. Wiley, New York, USA, pp. 1–29.
Taylor, B.E., 1986. Magmatic volatiles: isotopic variations of C, H, and S. Rev. Mineral. Geochem. 16, 185–225.
Tzvetanova, Y., 2003. Lead phosphate minerals from Brussevtzi Deposit (Eastern Rhodopes, Bulgaria) — SEM, IR and DTA studies. C. R. Acad. Bulg. Sci. 56, 55.
Vikre, P.G., 2007. Sinter–Vein correlations at Buckskin Mountain, National District, Humboldt County, Nevada. Econ. Geol. 102, 193–224.
Wallier, S., 2009. The geology and evolution of the Manantial Espejo epithermal silver (+gold) deposit, Deseado Massif, Argentina. Unpublished PhD Thesis. University of British Columbia, Vancouver, Canada. 303 pp. Available at: http://circle.ubc.ca/handle/2429/17439.
Wilkinson, J.J., 2001. Fluid inclusions in hydrothermal ore deposits. Lithos 55, 229–272.
Zheng, Y., 1993. Calculation of oxygen isotope fractionation in hydroxyl-bearing silicates. Earth Planet. Sci. Lett. 120, 247–263.